A thermo-mechanical constitutive model for fine-grained soils based on thermodynamics

Golchin, Ali; Vardon, Philip James; Hicks, Michael Anthony

Important note
To cite this publication, please use the final published version (if applicable).
Please check the document version above.

A thermo-mechanical constitutive model for fine-grained soils based on thermodynamics

Ali Golchin, Philip James Vardon [*], Michael Anthony Hicks

Section of Geoengineering, Department of Geoscience and Engineering, Delft University of Technology, the Netherlands

A B S T R A C T

The formulation of a new thermo-mechanical constitutive model consistent with the principles of thermodynamics is presented. The model is capable of predicting the rate-independent thermo-mechanical behavior of fine-grained soils. The constitutive equations are derived by defining only a Gibbs-type free energy and a dissipation potential, in accordance with the hyperplasticity method. The addition of thermo-elasticity to the energy potential, and the embedding of the identified thermo-mechanical mechanisms into a newly proposed dissipation potential, enables the model to describe the thermo-mechanical behavior. The proposed dissipation potential eliminates the application of shift stress, which results in a simpler formulation in the context of hyperplasticity. The step-by-step procedure of deriving the equations, as well as a detailed analysis of the parameters of the model, is presented. The performance of the model is shown to be in good agreement with experimental data. A qualitative description of the possible micro-scale mechanisms for fine-grained soils, when subjected to temperature variation, is presented, as a step towards including the mechanisms in the formulation.

1. Introduction

Recently, the application of thermo-active structures has gained attention in geotechnical projects. Energy-piles, thermal retaining walls and heat storage tanks are a few examples of geo-structures which exchange heat with the ground simultaneously with load-transfer (Brandl, 2006). Pipelines, radioactive waste disposal (Thomas, Vardon, & Cleall, 2014), etc., are other examples where thermo-mechanical behavior is important. As a result, thermally-induced stresses as well as mechanical loads are applied to the soil in contact with the structure. Concurrently, changes in temperature affect the mechanical and physical properties of the soil. It can be inferred that these effects, during the heat exchange process with the soil, may influence both the performance and safety of the geo-structure. Constitutive equations assigned to geomaterials in contact with thermo-active structures should contain the crucial aspects of the thermo-mechanical behavior of the geomaterial. A number of constitutive models have been developed to capture the thermo-mechanical behavior of soils (Abuel-Naga, Bergado, Bouazza, & Ramana, 2007; Cui, Potts, Zdravković, Gawecka, & Taborda, 2018; Cui, Sultan, & Delage, 2000; Di Donna & Laloui, 2015; Hamidi, Tourchi, & Kardooni, 2017; Hamidi, Tourchi, & Khazaei, 2015; Hong, Pereira, Cui, & Tang, 2016; Laloui & Cekerevac, 2003, 2008; Laloui, Cekerevac, & François, 2005; Laloui & François, 2009; Ma, Ng, Mašín, & Zhou, 2017; Mašín & Khalili, 2012; Xiong, Ye, Zhu, Zhang, & Zhang, 2016; Yao & Zhou, 2013; Zhou, Fong, & Ng, 2017; Zhou & Ng, 2015; Zhou and Ng, 2016). These models are mostly based on plasticity theory, and some are capable of capturing the

---

List of Symbols

Roman

$\mathbf{1}$	Identity tensor
A	Shape function for yield surface
a_k	Passive variables, $k=1,2,3,\ldots$
B	Shape function for yield surface
C	Shape function for yield surface
CSL	Critical State line
$\mathbf{C}^e$	Elastic compliance matrix
$\mathbf{D}^e$	Elastic stiffness matrix
d	Mechanical dissipation function
d^t	Total dissipation function
e	Void ratio
e_0	Initial void ratio
$\mathbf{e}^p$	Plastic deviatoric strain tensor
f	Helmholtz free energy potential
g	Gibbs free energy potential
g_1	Isothermal Gibbs free energy potential
$\overline{G}$	Maximum elastic shear modulus
h	Enthalpy
k_1,k_2	Functions
$\overline{K}$	Maximum elastic bulk modulus
l_1	Active variable
l_2	Conjugate of l_1
m	Power of p for bulk modulus
M	Critical State stress ratio
M_0	Critical State stress ratio at ambient temperature
n	Power of p for shear modulus
n_h	Order of a homogeneous function
NCL	Normal consolidation line
OCR	Over consolidation ratio
p	Mean effective stress
p_0	Initial mean effective stress
p_c	Pre-consolidation pressure
p_{cT}	Apparent pre-consolidation pressure
$\dot{p}_{cT}$	Rate of change of the apparent pre-consolidation pressure
p_{ref}	Reference mean effective stress
PI	Plasticity index
q	Deviatoric stress
$\boldsymbol{q}$	Heat flux vector
q_0	Initial deviatoric stress
$\dot{Q}$	Heat supply
r	Homogeneous function
r_p	Plastic flow in p direction
r_q	Plastic flow in q direction
$\mathbf{r}$	Plastic flow direction
RH	Rotational hardening
s	Entropy
$\dot{s}$	Rate of change of entropy
$\mathbf{s}$	Deviatoric stress tensor
t	Thickness of hydrate layers
u	Internal energy potential
$\dot{u}$	Rate of change of internal energy
u_p	Pore water pressure
$\mathbf{v}$	Generalized dissipative velocities
w	Flow potential
$\dot{W}$	Work input
$\mathbf{x}$	State variables

y	Yield function in true stress space
y^d	Yield function in dissipative stress space
$\dot{y}$	Rate of change of the yield function
z	Force potential
Greek	
α	Parameter related to the shape of the yield surface
α^*	Linear thermal expansion coefficient
$\boldsymbol{\alpha}_i$	Internal variables
β	Level of inclination of the yield surface
γ	Parameter related to the shape of the yield surface
$\boldsymbol{\varepsilon}$	Strain tensor
$\boldsymbol{\varepsilon}^p$	Plastic strain tensor
$\dot{\boldsymbol{\varepsilon}}$	Strain increment tensor
ε_v	Total volumetric strain
ε_s	Total deviatoric strain
ε_v^e	Elastic volumetric strain
ε_s^e	Elastic deviatoric strain
$\dot{\varepsilon}_v^e$	Elastic volumetric strain increment
$\dot{\varepsilon}_s^e$	Elastic deviatoric strain increment
ε_v^p	Plastic volumetric strain
ε_s^p	Plastic deviatoric strain
$\dot{\varepsilon}_v^p$	Plastic volumetric strain increment
$\dot{\varepsilon}_s^p$	Plastic deviatoric strain increment
ε_v^θ	Thermo-elastic volumetric strain
$\dot{\varepsilon}_v^\theta$	Thermo-elastic volumetric strain increment
η	Stress ratio
θ	Absolute temperature
θ_0	Initial absolute temperature
$\boldsymbol{\theta}_{,k}$	Thermal gradient
$\dot{\theta}$	Temperature increment
κ	Slope of unloading/reloading curve
λ	Slope of NCL
$\dot{\Lambda}$	Plastic multiplier
μ	Thermal softening coefficient
π	Coefficient of Critical State stress ratio variation with temperature
Π_t	Total disjoining pressure
Π_e	Electrostatic disjoining pressure
Π_m	Molecular disjoining pressure
Π_s	Structural disjoining pressure
$\boldsymbol{\sigma}$	Total stress tensor
$\dot{\boldsymbol{\sigma}}$	Stress increment tensor
$\boldsymbol{\sigma}'$	Effective stress tensor
Y	Scalar multiplier of $\boldsymbol{\chi}$
Y'	Scalar multiplier
$\overline{\chi}$	Generalized dissipative force
χ_p	Mean generalized dissipative stress
χ_q	Deviatoric generalized dissipative stress
$\overline{\boldsymbol{\chi}}$	Generalized stress
$\overline{\chi}_p$	Mean generalized stress
$\overline{\chi}_q$	Deviatoric dissipative stress

general thermo-mechanical behavior of soils with reasonable accuracy. However, mostly they do not follow the principles of thermodynamics; therefore, certain phenomena may not be captured/predicted and other phenomena may be spuriously predicted.

The principles of thermodynamics are sufficient to develop a framework which accurately captures the behavior of geomaterials (Houlsby & Puzrin, 2007; Srinivasa, 2010). To do so, the identification of the governing mechanisms during the process and the assigning of appropriate variables that represent the system are required. A discussion on selecting these variables can be found in Rajagopal & Srinivasa (2019). Several approaches exist that use the principles of thermodynamics to exploit constitutive equations (see Darabi, Abu Al-Rub, & Omidi (2018); Rajagopal & Srinivasa (2019), and Srinivasa (2010), for example). In this paper, a

thermo-mechanical constitutive model is developed, based on the thermodynamically-consistent framework of hyperplasticity. Hyperplasticity theory was firstly developed by Collins & Houlsby (1997), and combines and utilizes the laws of thermodynamics through the application of the maximum rate of dissipation, sometimes known as Ziegler's hypothesis (Ziegler, 1977). Thus, the derived constitutive equations satisfy the principles of thermodynamics and can be implemented with confidence into numerical simulations (Houlsby & Puzrin, 2007). This approach has been used to capture the creep and freezing of soils (Aung, Khabbaz, & Fatahi, 2019 and Lai, Liao, & Hu, 2016, respectively).

In Section 2 of the paper, the major aspects of the thermo-mechanical behavior of fine-grained soils are summarized, as observed from temperature-controlled element tests. A step-by-step procedure for deriving the constitutive equations of the thermo-mechanical model, including elasticity, the yield surface, the plastic flow rule, and the incremental formulation, from two potential functions, along with the procedure for calibrating the model parameters, is detailed in Section 3. A small-strain approach has been used here, as this constitutive model is designed to be included in a boundary value solver which follows an Updated Lagrangian approach for large strain problems (Bathe, Ramm, & Wilson, 1975); in addition, it allows easy comparison with other thermo-mechanical models available in literature. Care must be taken if using a boundary value simulator formulated using large (finite) strain, as the choice of objective rate impacts the formulation. An analysis of the general features of the model including the non-associated flow rule and energy conservation is given in Section 4, and this is followed by a detailed analysis of temperature effects in the constitutive equations in Section 5. The model is intensively validated by several temperature-controlled element tests in Section 6. Section 7 qualitatively describes the governing micro-scale mechanisms of fine-grained soils for different processes, in accordance with the findings of molecular and colloid chemistry theories, to explain the model choice made.

2. Thermo-mechanical behavior of fine-grained soils

In general, the mechanical response of materials can be investigated in two distinct parts: the volumetric behavior and the shear behavior. Similarly, the effect of temperature on the thermo-mechanical behavior of soils can be split into thermally-induced volumetric and thermally-induced shear effects.

Normally and slightly over-consolidated clayey-soils (soils with low over-consolidation ratios) undergo permanent volumetric contraction when they are subjected to an increase in temperature (Abuel-Naga, Bergado, & Bouazza, 2007a; Cekerevac & Laloui, 2004; Di Donna & Laloui, 2015; Sultan, Delage, & Cui, 2002; Towhata, Kuntiwattanaku, Seko, & Ohishi, 1993; Uchaipichat & Khalili, 2009). As the over-consolidation ratio (OCR) increases, the severity of the thermally-induced volumetric contraction decreases and, at high OCRs, the thermo-mechanical behavior transitions to volumetric expansion. This volumetric expansion is mostly reversible and is attributed to the thermo-elasticity of highly over-consolidated soils due to the volumetric expansion of soil particles without rearrangement (Khalili, Uchaipichat, & Javadi, 2010).

Soils also show a reduction in yielding stress (represented by pre-consolidation pressure) at higher temperatures, when
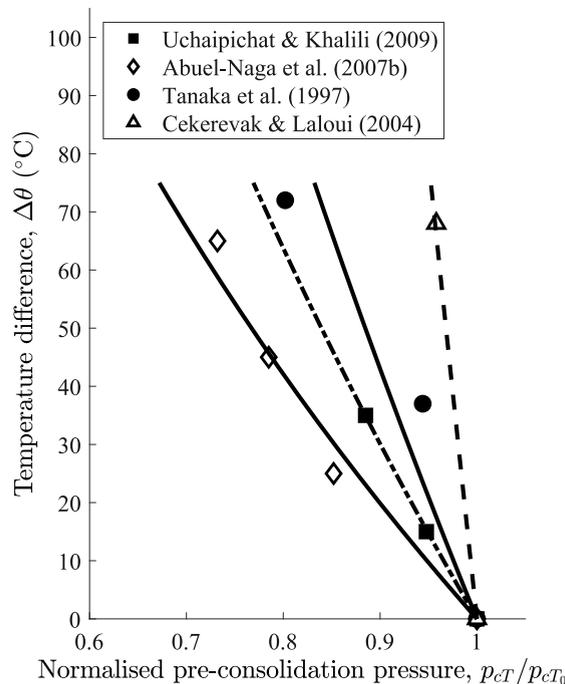

Fig. 1. Reduction of the normalized pre-consolidation pressure with temperature difference $\Delta\theta°$C.

consolidated isotropically (Abuel-Naga, Bergado, Bouazza, 2007a; Cekerevac & Laloui, 2004; Tanaka, Graham, & Crilly, 1997; Uchaipichat & Khalili, 2009). Variation of the pre-consolidation pressure at different temperatures (p_{cT}), normalized by the pre-consolidation pressure at the ambient temperature (p_{cT0}), with respect to the subjected temperature difference, is shown in Fig. 1 for different soils.

On the other hand, the shear behavior of soils shows a range of behaviors as the temperature is elevated. Depending on the mineralogy and constituents of the soil, the peak shear strength and dilatancy may increase, remain unchanged, or decrease during heating (Abuel-Naga, Bergado, & Lim, 2007c; Cekerevac & Laloui, 2004; Hueckel & Baldi, 1991; Hueckel, François, & Laloui, 2009; Kuntiwattanakul, Towhata, Ohishi, & Seko, 1995; Ng, Cheng, Zhou, & Alonso, 2016). A similar result has also been reported for the stress ratio at Critical State conditions (Abuel-Naga, Bergado, & Lim, 2007c; Cekerevac & Laloui, 2004; Ghahremannejad, 2003; Tanaka *et al.*, 1997; Uchaipichat & Khalili, 2009) (see Fig. 2). A reduction or increase in the elastic shear modulus observed at elevated temperatures is another demonstration of mineralogy-dependency of the shear behavior of soils (Zhou, Xu, & Ng, 2015).

Soils exhibit hardening behavior during heating-cooling cycles (Bai & Su, 2012; Di Donna & Laloui, 2015; Ng *et al.*, 2016; Vega & McCartney, 2015). The oedometer test results for two different clays (Abuel-Naga, Bergado, & Bouazza, 2007a; Towhata *et al.*, 1993), subjected to a heating-cooling cycle (heating followed by cooling), are presented in Fig. 3. During the heating-cooling cycle, the void ratio reduces (permanent volumetric strains produced), leading toward a denser state. As a result, the pre-consolidation pressure increases and the elastic domain becomes bigger.

When soils are subjected to several thermal cycles, each cycle adds to the accumulated permanent volumetric strain. However, the amount of permanent strain in a cycle reduces with consecutive cycles, until a thermally stable condition is reached. In this condition, the permanent component of volumetric strain tends to zero and the behavior becomes totally elastic, governed by the volumetric thermal expansion of soil grains.

The structure and chemical-reactivity potential of a soil are proven to significantly affect the intensity-level of thermally induced deformation during heating (Abuel-Naga *et al.*, 2006; Laloui, Leroueil, & Chalindar, 2008; Ng *et al.*, 2016; Sultan *et al.*, 2002; Vega & McCartney, 2015). The plasticity index, PI, can be considered as an indication of the level of chemical-reactivity potential. As the PI increases, the soil is more susceptible to permanent volumetric reduction at elevated temperatures (Di Donna & Laloui, 2015; Hueckel & Baldi, 1991). Also, normally and slightly consolidated intact soils, with randomly distributed size and position of void spaces, are susceptible to higher volumetric contraction in comparison to remolded soil specimens with uniformly distributed voids (both in size and position) (Ng *et al.*, 2016).
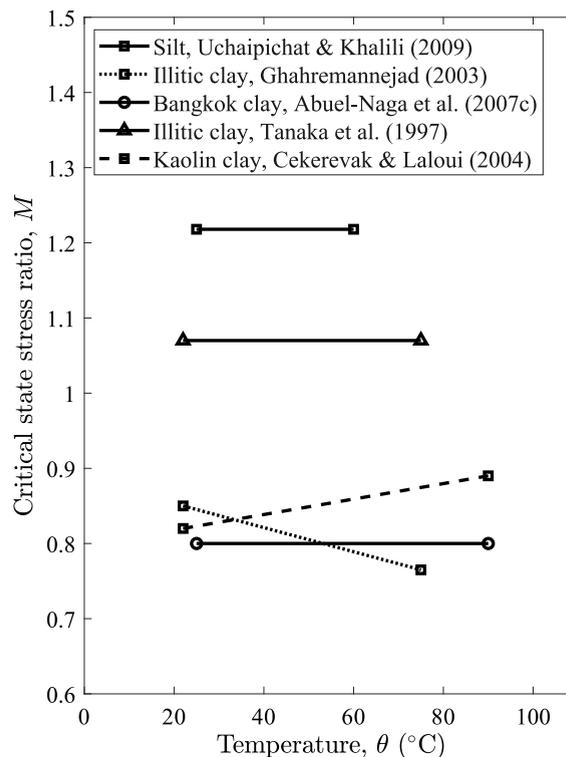

Fig. 2. Variation of Critical State stress ratio, *M*, with temperature θ °C.
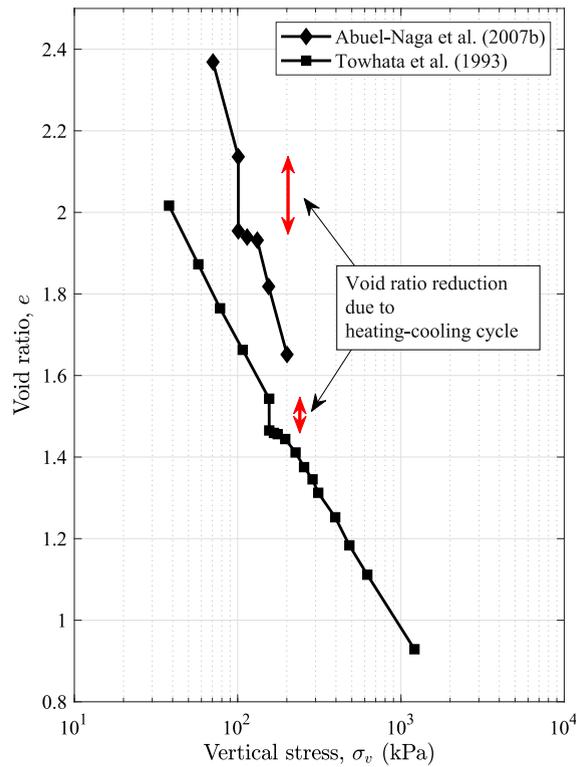
Fig. 3. Hardening behavior during heating-cooling cycle.

3. Formulation of the thermo-mechanical model

To capture the thermo-mechanical behavior of soils, it is here proposed that the thermo-mechanical behavior be defined using Terzaghi's effective stress, by embedding thermal mechanisms into the constitutive formulation. Terzaghi's (1925) effective stress tensor is defined as:

$$\boldsymbol{\sigma}' = \boldsymbol{\sigma} - u_p \mathbf{1} \tag{1}$$

where $\boldsymbol{\sigma}$ and u_p are the total stress tensor and pore pressure, respectively, and $\mathbf{1}$ is the second order identity tensor, and the effective stress is proven to be a thermodynamically consistent stress state variable that can reflect the mechanical behavior of saturated soils (Houlsby, 1997). From here on, all the stresses are effective. The employed continuum-scale thermo-mechanical mechanisms in this model are outlined as follows:

1. The position of the total (or permanent) volume variation due to change in the mean effective stress (p) line (often referred to as the normal consolidation line (NCL)) changes with temperature.
2. The gradients of elastic and permanent volume variations due to changes in mean effective stress (p) are insensitive to temperature variation.
3. The bounded size of the elastic domain changes as the temperature varies (Eq. 13).
4. The shear strength (i.e. the stress ratio) at the Critical State conditions may change (increase, decrease or remain constant) as temperature varies (Eq. 12).
5. Thermal expansion of soil grains is thermo-elastic (Eq. E-5).

The components of the model, including elasticity, plasticity, and flow and hardening rules, are determined by specifying two potentials; namely, the Gibbs free energy potential and the dissipation potential. The yield surface in the Meridian plane has an ellipsoid-type shape (demonstrated to be appropriate for geomaterials Collins & Hilder (2002)) and is defined by two parameters. It has the capability to rotate (be inclined with respect to the p-axis) and expand or shrink in the presence of isotropic hardening. The plastic flow (direction of the plastic strain increments) is non-associated, but without the necessity of defining a separate plastic potential as is the case in conventional plasticity models.

The major temperature effects on the mechanical behavior of fine-grained soils, explained in Section 2, are associated with the irreversible response of the material. The variation of the apparent pre-consolidation pressure, p_{cT}, and the Critical State stress ratio, M,

with temperature, respectively, represents the temperature influence on the variation of the yielding stress (initiation of irreversible response) and friction angle when the shear strength is fully mobilized (ultimate shear strength). Since the plasticity component of the constitutive equations are directly derived from the dissipation potential, it is logical to incorporate the identified thermo-mechanical mechanisms into the dissipation potential. By this, and with the addition of a volumetric thermal expansion component in the Gibbs free energy potential (to capture the thermo-elasticity), the temperature effects on both the volumetric and shear behaviors of soils are captured.

A new dissipation potential is proposed, which not only embeds the thermo-mechanical mechanisms, but also omits the utilization of shift stresses during the conversion from dissipation space to true stress space (see Appendix A); i.e., the addition of a kinematic hardening to shift the yield surface is excluded. Consequently, a simpler formulation is derived, which simplifies its numerical implementation in boundary value solvers such as the finite element and material point methods.

In the following, the procedure of deriving the complete constitutive formulation within the framework of hyperplasticty is presented. To the best knowledge of the authors, the current model is the first thermo-mechanical model for fine-grained soils developed by this framework. For completion, a description of the hyperplasticty approach is provided in Appendix A.

3.1. Energy potential including temperature effects

A Gibbs-type function is proposed for the free energy potential and is defined by true stress invariants in triaxial stress space (mean effective stress, $p=tr(\boldsymbol{\sigma})/3$ (kPa) and deviatoric stress, $q=(3/2 \ \mathbf{s:s})^{1/2}$ (kPa), where $\mathbf{s}=\boldsymbol{\sigma}-tr(\boldsymbol{\sigma})/3\mathbf{:1}$ is the deviatoric stress tensor), internal variables (which here are only the plastic strain invariants; the plastic volumetric strain, $\varepsilon_v{}^p=tr(\boldsymbol{\varepsilon}^p)$, and the plastic deviatoric strain, $\varepsilon_s{}^p=(2/3 \ \mathbf{e}^p\mathbf{:e}^p)^{1/2}$; $\mathbf{e}^p=\boldsymbol{\varepsilon}^p-tr(\boldsymbol{\varepsilon}^p)/3\mathbf{:1}$, where $\boldsymbol{\varepsilon}^p$ and $\mathbf{e}^p$ are plastic strain and plastic deviatoric strain tensors, respectively), and the absolute temperature θ (K), as the independent variables:

$$g\left(p,q,\varepsilon_v^p,\varepsilon_s^p,\theta\right) = g_1(p,q) - p\varepsilon_v^p - q\varepsilon_s^p - 3\alpha^*p(\theta-\theta_0) \tag{2}$$

where α^* is the linear thermal expansion coefficient of the soil skeleton. Note that this formulation is based upon small-strain assumptions, and different conjugate pairs are required for large strain formulations. The term $3\alpha^*p(\theta-\theta_0)$ represents the isotropic thermal volumetric expansion of the elasticity, due to temperature variation (thermo-elasticity). The linear thermal expansion coefficient α^* is considered constant, although its dependency on temperature, stress level and over-consolidation ratio has been addressed in literature. A constant value of α^*, with respect to both temperature and stress level, ensures thermodynamical consistency. Anisotropic terms for the thermal expansion coefficient for thermo-elasticity can be used if desired, although further experimental support is needed to define the appropriate terms.

The form of the energy potential in Eq. 2 leads to a "decoupled" material behavior (Collins & Houlsby, 1997), through the terms $p\varepsilon_v^p$ and $q\varepsilon_s^p$, in which the elastic and plastic behaviors are independent of each other. Energy potentials incorporating elastic-plastic coupling can be found in the works of Collins (2002), Golchin & Lashkari (2014), and Lashkari & Golchin (2014), which result in a complex elasticity formulation. For the sake of simplicity, and due to the lack of evidence linking the plasticity to the elasticity of fine-grained soils, decoupled behavior is considered here. The term $g_1(p,q)$ is the free energy function for isothermal conditions, previously proposed by Einav & Puzrin (2004) for geomaterials, in which the elasticity component of the model (for isothermal conditions) is derived as:

$$g_1(p,q) = -\frac{p^{2-m} - (2-m)pp_0^{1-m}}{\overline{K}(2-m)(1-m)p_{ref}^{1-m}} - \frac{q^2}{6\overline{G}p_{ref}^{1-n}p^n} + \frac{q_0(2qp_0 - nq_0p)}{6\overline{G}p_{ref}^{1-n}p_0^{1+n}} \tag{3}$$

where p_{ref} (kPa) is the reference pressure (normally 1 kPa); p_0 and q_0 are the initial values of the mean effective and deviatoric stresses, respectively; $\overline{K}$ and $\overline{G}$ are material constants, respectively related to the elastic bulk modulus and shear modulus; and m and n are constants representing the power dependence of the bulk and shear moduli, respectively, on the mean effective stress p. For the case when the bulk modulus is linearly proportional to p (for cases in which $m=1$), the free energy is natural-log dependent on p:

$$g_1(p,q) = -\frac{p}{\overline{K}}\left(\ln\left(\frac{p}{p_0}\right)-1\right) - \frac{q^2}{6\overline{G}p_{ref}^{1-n}p^n} + \frac{q_0(2q-nq_0p)}{6\overline{G}p_{ref}^{1-n}p_0^n} \tag{4}$$

Following Eq. A-7, the total strains ($\varepsilon_v, \varepsilon_s$), consisting of elastic ($\varepsilon_v^e, \varepsilon_s^e$), thermo-elastic ($\varepsilon_v^\theta$), and thermo-plastic components ($\varepsilon_v^p, \varepsilon_s^p$), are derived by differentiating the free energy potential (Eq. 2) with respect to the stress components (p, q):

$$\varepsilon_v = -\frac{\partial g\left(p,q,\varepsilon_v^p,\varepsilon_s^p,\theta\right)}{\partial p} = -\frac{\partial g_1(p,q)}{\partial p} + 3\alpha^*(\theta-\theta_0) + \varepsilon_v^p = \varepsilon_v^e + \varepsilon_v^\theta + \varepsilon_v^p \tag{5}$$

$$\varepsilon_s = -\frac{\partial g\left(p,q,\varepsilon_v^p,\varepsilon_s^p,\theta\right)}{\partial q} = -\frac{\partial g_1(p,q)}{\partial q} + \varepsilon_s^p = \varepsilon_s^e + \varepsilon_s^p \tag{6}$$

Since the thermal expansion (i.e. the term $3\alpha^*p(\theta-\theta_0)$ in Eq. 2) is only defined for the volumetric part of the energy potential (isotropic term), the deviatoric thermo-elastic strain is zero. In summary, the total strain can be rewritten in compact format as:

$$\left\{ \begin{array}{c} \varepsilon_v \\ \varepsilon_s \end{array} \right\} = \left\{ \begin{array}{c} \varepsilon_v^e \\ \varepsilon_s^e \end{array} \right\} + \left\{ \begin{array}{c} \varepsilon_v^\theta \\ 0 \end{array} \right\} + \left\{ \begin{array}{c} \varepsilon_v^p \\ \varepsilon_s^p \end{array} \right\}$$

where $\varepsilon_v^e = -\frac{\partial g_1(p,q)}{\partial p}; \varepsilon_s^e = -\frac{\partial g_1(p,q)}{\partial q}; \varepsilon_v^\theta = 3\alpha^*(\theta - \theta_0)$.

The generalized stresses (see Appendix A), i.e. the derivative of the Gibbs free energy potential with respect to internal variables, are:

$$\left\{ \begin{array}{c} \overline{\chi}_p \\ \overline{\chi}_q \end{array} \right\} = -\left\{ \begin{array}{c} \frac{\partial g}{\partial \varepsilon_v^p} \\ \frac{\partial g}{\partial \varepsilon_s^p} \end{array} \right\} = \left\{ \begin{array}{c} p \\ q \end{array} \right\} \tag{7}$$

3.2. Dissipation potential including temperature effects

In order to determine the plastic strains of a rate-independent material, the definition of an appropriate dissipation potential function is required. Collins & Hilder (2002) proposed a dissipation potential for fine-grained soils and connected it to the conjugated energy potential through the shift stress. Here, a new dissipation potential is presented whose novelty is twofold. Firstly, the dissipation function is defined in such a way so that the use of the shift stress is eliminated, while preserving the properties of the dissipation potential in Collins & Hilder (2002) (with the advantage of a simpler formulation in comparison to the equations in Collins & Hilder (2002)) and secondly, it incorporates the continuum-scale thermal mechanisms which are encapsulated in the apparent pre-consolidation pressure and Critical State stress ratio. The dissipation function is defined as:

$$d = C\left(\dot{\varepsilon}_v^p + \beta\dot{\varepsilon}_s^p\right) + \sqrt{A^2\left(\dot{\varepsilon}_v^p + \beta\dot{\varepsilon}_s^p\right)^2 + B^2\left(\dot{\varepsilon}_s^p\right)^2} \tag{8}$$

where $\dot{\varepsilon}_v^p$ and $\dot{\varepsilon}_s^p$ are plastic volumetric and deviatoric strain increments (as the generalized dissipative velocities, or the rate of change of internal variables in the case of rate-independent behavior (see Appendix A), respectively; and β represents the level of anisotropy by inclining the yield surface with respect to the p-axis. A, B and C are functions defined by stress, history and shape parameter components, which define the shape and size of the yield function (to be determined later). Readers are referred to Collins & Hilder (2002) for the procedure of determining the functions A and B. These two functions, with the newly defined function C, are defined as:

$$A = (1-\gamma)p + \frac{\gamma}{2}p_{cT} \tag{9}$$

$$B = M\left((1-\alpha)p + \frac{\alpha\gamma}{2}p_{cT}\right) \tag{10}$$

$$C = \frac{\gamma}{2}p_{cT} \tag{11}$$

where α and γ are parameters that affect the shape of the yield surface. These two parameters provide the benefit of defining a single yield surface, resembling a Hvorslev-type surface for highly over-consolidated stress states and a cap-type surface for normally and lightly consolidated states. This can overcome the over-prediction of shear strength for highly over-consolidated soils that has been observed when using Modified Cam Clay-type models. M is the stress ratio at the Critical State. It has been seen in Fig. 2 that M may change due to temperature variation. In this regard, a linear variation with temperature (as a first approximation) is considered:

$$M = M_0 + \pi(\theta - \theta_0) \tag{12}$$

where π is the slope of the variation of M with respect to temperature θ, and M_0 is the Critical State stress ratio at ambient temperature. The value of π depends on the mineralogy of the soil; M may increase or decrease with temperature, so that π may take positive or negative values, respectively, and in the case of temperature independency its value is zero.

p_{cT} is the apparent pre-consolidation pressure, which for the isothermal condition (no temperature variation) is similar to the formulation presented in Houlsby & Puzrin (2007) and Puzrin (2012). Here, the effect of temperature (see Fig. 1) is included in the pre-consolidation pressure as follows:

$$p_{cT} = p_{c0}e^{\frac{1+e_0}{\lambda-\kappa}\varepsilon_v^p}\ e^{-\mu(\theta-\theta_0)} \tag{13}$$

where p_{c0} is the initial pre-consolidation pressure; λ and κ are the slopes of the normal compression (NCL) and unloading lines in $\ln e$ (void ratio), versus $\ln p$ space, respectively; e_0 and θ_0 are the initial void ratio and ambient absolute temperature, respectively; and μ is the coefficient of thermal softening, first presented by Cui et al. (2000). The apparent pre-consolidation pressure hardens isotropically with plastic volumetric strain (through the term $e^{((1+e_0)/(\lambda-\kappa))\varepsilon_v^p}$), while it (thermally) softens with an increase in temperature (through the term $e^{-\mu(\theta-\theta_0)}$). Thermal softening influences (i.e. reduces) the size of the elastic domain and represents the thermal mechanism

proposed for the volumetric part of the behavior of soils.

Since the above dissipation potential is defined for rate-independent materials, it is identical to the force potential z (see Appendix A). Hence, the yield function (surface) can be derived, as defined by the generalized dissipative forces (or dissipative stresses in the case of rate-independent materials) which are determined as the derivation of the dissipation potential function with respect to the rate of internal variables (Eq. A-15). The dissipative stresses are:

$$\left\{ \begin{array}{c} \chi_p \\ \chi_q \end{array} \right\} = \left\{ \begin{array}{c} \frac{\partial d}{\partial \dot{\varepsilon}_v^p} \\ \frac{\partial d}{\partial \dot{\varepsilon}_s^p} \end{array} \right\} = \left\{ \begin{array}{c} C + \dfrac{A^2\left(\dot{\varepsilon}_v^p + \beta\dot{\varepsilon}_s^p\right)}{\sqrt{A^2\left(\dot{\varepsilon}_v^p + \beta\dot{\varepsilon}_s^p\right)^2 + B^2\left(\dot{\varepsilon}_s^p\right)^2}} \\ \beta C + \dfrac{B^2\dot{\varepsilon}_s^p + \beta A^2\left(\dot{\varepsilon}_v^p + \beta\dot{\varepsilon}_s^p\right)}{\sqrt{A^2\left(\dot{\varepsilon}_v^p + \beta\dot{\varepsilon}_s^p\right)^2 + B^2\left(\dot{\varepsilon}_s^p\right)^2}} \end{array} \right\} \tag{14}$$

The general procedure for deriving the yield surface for rate-independent materials, where the dissipation potential is a first order homogenous function of plastic strain rates, is by invoking the Legendre-Fenchel transform on the dissipation function, since the classical Legendre transform becomes degenerate (Srinivasa, 2010). However, this procedure can also be done in a simpler way. Any mathematical equation consisting of the dissipative stresses in Eq. 14 that equals to zero represents the yield function. Hence, the yield function is:

$$y^d = B^2\left(\chi_p - C\right)^2 + A^2\left(\chi_q - \beta\chi_p\right)^2 - A^2B^2 = 0 \tag{15}$$

This form of yield function indicates an ellipsoid and is defined in dissipative stress space (χ_p, χ_q), rather than in conventional stress space (p, q). The yield function may be transferred to true stress space (see Appendix A) by ensuring the maximum rate of dissipation.

3.3. Temperature dependent flow rule

The flow of plastic strain increments is always normal to the yield surface (y^d) in dissipative stress space (Collins & Houlsby, 1997; Houlsby & Puzrin, 2007), i.e., the flow rule is always associated in dissipative stress space. This can be mathematically shown as the derivative of the yield surface y^d (Eq. 15) with respect to dissipative stresses as:

Table 1

Comparison between the yield surface defined in dissipative stress space and that defined in true stress space, along with their respective normal, and the flow rule in true stress space.

Yield surface defined in dissipative stress space (χ_p and χ_q) (Eq. 15)	Yield surface defined in true stress space (p and q) (Eq. 18)
$y^d = B^2(\chi_p - C)^2 + A^2(\chi_q - \beta\chi_p)^2 - A^2B^2 = 0$ (T-1)	$y = B^2(p - C)^2 + A^2(q - \beta p)^2 - A^2B^2 = 0$ (T-4)
Derivative of y^d with respect to dissipative stresses (χ_p and χ_q) (associated flow rule in dissipative stress space (Eq. 16))	Derivative of y with respect to true stresses (p and q) (normal to the yield surface)
$\left\{ \begin{array}{c} \frac{\partial y^d}{\partial \chi_p} \\ \frac{\partial y^d}{\partial \chi_q} \end{array} \right\} = 2\left\{ \begin{array}{c} B^2(\chi_p - C) - \beta A^2(\chi_q - \beta\chi_p) \\ A^2(\chi_q - \beta\chi_p) \end{array} \right\}$ (T-2)	$\left\{ \begin{array}{c} \frac{\partial y}{\partial p} \\ \frac{\partial y}{\partial q} \end{array} \right\} = \left\{ \begin{array}{c} r_p + \frac{\partial y}{\partial A}\frac{\partial A}{\partial p} + \frac{\partial y}{\partial B}\frac{\partial B}{\partial p} \\ r_q + \frac{\partial y}{\partial A}\frac{\partial A}{\partial q} + \frac{\partial y}{\partial B}\frac{\partial B}{\partial q} \end{array} \right\}$ (T-5)
Flow rule in true stress space (Eq. 19) (by applying the criterion of maximizing the rate of dissipation, Eq. 17, to the associated flow rule in dissipative stress space (T-2))	where r_p and r_q are defined in (T-3)
maximum rate of dissipation criteria $\longrightarrow$ $\left\{ \begin{array}{c} \chi_p \\ \chi_q \end{array} \right\} = \left\{ \begin{array}{c} p \\ q \end{array} \right\}$ (Eq.17) {Flow direction} $= \left\{ \begin{array}{c} r_p \\ r_q \end{array} \right\} = 2\left\{ \begin{array}{c} B^2(p - C) - \beta A^2(q - \beta p) \\ A^2(q - \beta p) \end{array} \right\}$ (T-3)	

$$\left\{ \begin{array}{c} \dot{\varepsilon}_v^p \\ \dot{\varepsilon}_s^p \end{array} \right\} = \dot{\Lambda} \left\{ \begin{array}{c} \dfrac{\partial y^d}{\partial \chi_p} \\[2mm] \dfrac{\partial y^d}{\partial \chi_q} \end{array} \right\} = 2\dot{\Lambda} \left\{ \begin{array}{c} B^2 (\chi_p - C) - \beta A^2 (\chi_q - \beta \chi_p) \\ A^2 (\chi_q - \beta \chi_p) \end{array} \right\} \tag{16}$$

where $\dot{\Lambda}$ is the plastic multiplier defining the plastic strain increment magnitude.

One of the useful assumptions implemented into hyperplasticity theory is the criterion of maximizing the rate of dissipation (see Appendix A), which is used to link the generalized stress (Eq. 7) to the dissipative stress (Eq. 14). By the use of Eq. 7 and Eq. A-10, the generalized dissipative stress becomes:

$$\left\{ \begin{array}{c} \chi_p \\ \chi_q \end{array} \right\} = \left\{ \begin{array}{c} p \\ q \end{array} \right\} \tag{17}$$

This outcome results in the definition of both the yield surface (Eq. 15) and plastic flow (Eq. 16) in conventional stress space (p, q), by substituting the dissipative stresses with generalized stresses (as in Eq. 17). Consequently, the yield surface and plastic flow in terms of true stresses respectively become:

$$y = B^2 (p - C)^2 + A^2 (q - \beta p)^2 - A^2 B^2 = 0 \tag{18}$$

$$\left\{ \begin{array}{c} \dot{\varepsilon}_v^p \\ \dot{\varepsilon}_s^p \end{array} \right\} = \dot{\Lambda} \left\{ \begin{array}{c} r_p \\ r_q \end{array} \right\} = 2\dot{\Lambda} \left\{ \begin{array}{c} B^2 (p - C) - \beta A^2 (q - \beta p) \\ A^2 (q - \beta p) \end{array} \right\} \tag{19}$$

It should be noted that the plastic flow in dissipative stress space Eq. 16) is associated to the yield surface y^d (Eq. 15) with respect to the dissipative stresses χ_p and χ_q. However, the plastic flow in true stress space (Eq. 19) becomes non-associated with respect to the yield surface y defined in true stress space (Eq. 18). This is due to the true stress-dependency of the dissipation function via functions A and B (see Eqs. 9-10). Table 1 presents the yield surfaces defined in dissipative stress space and true stress space, along with their respective derivatives, and the flow rule in true stress space. The flow rule and normal to the yield surface ((T-3) and (T-5), respectively) are different, as in true stress space the stress dependency of functions A and B are included in (T-5), whereas they are not in (T-3). An associated flow rule (in true stress space) would include this dependency, i.e. would follow (T-5); hence, (T-3) indicates the non-associativity of the plastic flow in true stress space. This is compatible with the findings of Rajagopal & Srinivasa (2019) and Srinivasa (2010), where it was shown that the non-associated flow rule for frictional materials (i.e. pressure-dependent materials such as geomaterials) is the result of the dependency of the dissipation function to stresses.

The non-associated plastic flow presented above, unlike classical plasticity theory, is derived without the necessity of introducing a separately defined plastic potential. Srinivasa (2010) showed that for a dissipation function defined by separable functions of stress and plastic strain increments, i.e., having the form of $d = d_1(\boldsymbol{\sigma}) d_2(\dot{\boldsymbol{\varepsilon}}^p)$, it is possible to derive the plastic potential (as well as the yield surface). Note that the dissipation function adopted here (Eq. 8) is not defined as a separable function. Thus, it may not be straightforward to determine the plastic potential in true stress space, although the plastic flow (Eq. 19 or Eq. T-3) is derived.

3.4. Temperature dependent hardening rules

In strain hardening hyperplasticity models, the hardening rules are specified by the potential functions. The proposed model consists of an isotropic hardening rule and may be extended to account for rotational hardening (though not covered in this paper). The isotropic hardening is embedded through the way that the dissipative function is defined, by making the dissipative function dependent on internal variables (which here is the plastic volumetric strain).

3.4.1. Isotropic hardening

The apparent pre-consolidation pressure p_{cT} is the isotropic hardening variable of the model. It hardens by plastic volumetric strain increments (similar to the MCC family of models), while it softens by an increase in temperature (Eq. 13). By determining the rate of Eq. 13 (differentiation with respect to plastic volumetric strain ε_v^p, and absolute temperature θ), the isotropic hardening is derived:

$$\dot{p}_{cT} = \left(\frac{1 + e_0}{\lambda - \kappa} \dot{\varepsilon}_v^p - \mu \dot{\theta} \right) p_{cT} \tag{20}$$

3.4.2. Rotational hardening

Although various rotational hardening (RH) rules for clay constitutive models exist in literature (Coombs, Crouch, & Augarde, 2013; Dafalias & Taiebat, 2013, 2014; Nieto-Leal, Kaliakin, & Mashayekhi, 2018; Wheeler, Näätänen, Karstunen, & Lojander, 2003), RH is not considered in this model. Several issues may arise regarding RH, so that its implementation should be considered with caution. For example, assigning RH may lead to a unique or non-unique anisotropic Critical State, which is a debateable issue (Dafalias & Taiebat, 2014) and beyond the scope of this paper. Also, it may not be possible to determine a thermodynamically-consistent RH rule that is simultaneously compatible with currently accepted RH rules and criteria. This implies that further investigation is required to

define an appropriate RH rule that is thermodynamically-consistent while matching with experimental data. However, here the yield surface is capable of being inclined in p-q stress space through the parameter β. This may be useful to capture the anisotropic shape of the yield surface for soils that have previously been anisotropically loaded, e.g. under K_0 conditions.

3.5. Temperature dependent plastic multiplier

The last component of this model that needs to be determined is the plastic multiplier, representing the magnitude of the plastic strain increments. Eq. 18 can be written in the general form, $y = y(p, q, \varepsilon_v^p, \theta)$. The consistency condition can then be written as:

$$\dot{y} = \left\{ \frac{\partial y}{\partial p} \quad \frac{\partial y}{\partial q} \right\} \cdot \left\{ \begin{array}{c} \dot{p} \\ \dot{q} \end{array} \right\} + \left\{ \frac{\partial y}{\partial \varepsilon_v^p} \quad 0 \right\} \cdot \left\{ \begin{array}{c} \dot{\varepsilon}_v^p \\ \dot{\varepsilon}_q^p \end{array} \right\} + \frac{\partial y}{\partial \theta} \dot{\theta} = 0 \tag{21}$$

By substitution of Eq. 19 into Eq. 21, the plastic multiplier can be determined as:

$$\dot{\Lambda} = -\frac{\left\{ \frac{\partial y}{\partial p} \quad \frac{\partial y}{\partial q} \right\} \cdot \left\{ \begin{array}{c} \dot{p} \\ \dot{q} \end{array} \right\} + \frac{\partial y}{\partial \theta} \dot{\theta}}{\left\{ \frac{\partial y}{\partial \varepsilon_v^p} \quad 0 \right\} \cdot \left\{ \begin{array}{c} r_p \\ r_q \end{array} \right\}} = -\frac{\left\{ \frac{\partial y}{\partial \boldsymbol{\sigma}} \right\}^{\mathrm{T}} \{\dot{\boldsymbol{\sigma}}\} + \frac{\partial y}{\partial \theta} \dot{\theta}}{\left\{ \frac{\partial y}{\partial \dot{\boldsymbol{\varepsilon}}^p} \right\}^{\mathrm{T}} \{\mathbf{r}\}} \tag{22}$$

The components of this formulation can be found in Appendix D.

3.6. Incremental formulation

For numerical analysis, an incremental relationship between stress and strain is mostly utilized. The incremental formulations can be derived based on stress or strain controlled conditions (as the input); both scenarios can be found in Appendix E.

3.7. Parameters of the model

Depending on which energy potential for elasticity is chosen (Eq. 3 or Eq. 4), the model is defined by 12 or 11 parameters, respectively. These parameters can be categorzed in accordance to their role in the behavior of the material; volumetric behavior (elastic and plastic), shear behavior (elastic and plastic), temperature impacts, and parameters related to the shape of the yield surface. The relevant parameters in each category and the required tests for determining them are summarized in Table 2. Rotation of the yield surface, controlled by β, is not considered ($\beta=0$).

$\overline{K}$, $\overline{G}$, m and n are material constants related to elastic properties. $\overline{K}$ and $\overline{G}$ are attributed to the maximum values of the bulk and shear moduli of the soil, respectively. They can be determined from the tangential values of the p-ε_v and q-ε_s curves, respectively, at low strain levels (representing the elastic region). These parameters can be measured from drained triaxial tests or more accurately from resonant column and bender element tests. The parameters m and n are the powers related to p for the elastic bulk and shear moduli. In the case of $m=n=1$, where the elastic bulk and shear moduli are linearly dependent on p, the number of parameters reduces to 10.

λ and κ are related to the volumetric behavior of soils and are, respectively, the negative slopes of the normal compression and swelling lines in $\ln e$-$\ln p$ space, measured from isotropic triaxial (at $q=0$) consolidation or oedometer tests.

M_0 is the stress ratio (q/p) at the Critical State conditions at ambient temperature. It can be measured as the slope of a line passing

Table 2
Parameters of the model.

Categories		Parameters	Required tests
Volumetric behavior	Elastic	$\overline{K}$, m	Resonant column test, bender element test or triaxial test
	Elastic	κ	Triaxial consolidation or oedometer tests
	Plastic	λ	Triaxial consolidation or oedometer tests
Shear behavior	Elastic	$\overline{G}$, n	Resonant column test, bender element test or triaxial test
	Plastic	M_0	Triaxial test
Temperature effects		π, μ, α^*	Series of temperature-controlled triaxial tests
Related to yield surface shape		α, γ	Series of triaxial tests

through the final stress ratio of a soil monotonically loaded to the Critical State conditions, e.g. as determined from both drained and undrained triaxial tests, and the origin (q=p=0) in p-q stress space.

π can be determined as the ratio of the change in Critical State stress ratio to the change in temperature (from Eq. 12), $\pi = (M_{\theta_2} - M_{\theta_1})/(\theta_2 - \theta_1)$. Thus, triaxial tests at two temperatures would be sufficient. μ can be calculated from Eq. 13 as $\mu = -\ln(p_{cT}/p_c)/(\theta - \theta_0)$. Thus, by using 2 triaxial tests with equal pre-consolidation pressures at two different temperatures, the thermal softening coefficient may be determined.

As explained in Section 2, when fine-grained soils are subjected to heating-cooling cycles, they may show a hardening behavior by undergoing permanent volumetric contraction until they reach a thermally-stable condition and further volumetric behavior becomes thermally elastic. Therefore, any change in volumetric strain with respect to temperature (in θ-ε_v space) is attributed to the volumetric thermal expansion coefficient, $3\alpha^*$, and can be approximated as $3\alpha^* = \Delta\varepsilon_v/\Delta\theta$, where $\Delta\varepsilon_v$ is the change in volumetric strain. A sample in a triaxial test setup subjected to equal-amplitude temperature cycles is sufficient; the test must be run until the cycles give converged results.

The yield surface of the model may be adjusted to different yield loci reported for a wide variety of soils via parameters α and γ. By trial and error, it is possible to match the desired shape of the yield surface. Typically, at least 3 triaxial tests are needed to determine the yield surface; one almost normally consolidated, one lightly over-consolidated and the third, highly over-consolidated.

4. Features of the model

One of the interesting features of the model is that a non-associated flow rule (Eq. 19) is derived without the necessity to introduce an additional potential, e.g. the plastic potential as in conventional plasticity theory. Yield surfaces with different α values with γ=1, as examples, are plotted with their corresponding plastic flow directions in Fig. 4. It is obvious that in none of the cases (except for α=γ=1 in which the dissipation function becomes stress independent) is the plastic flow direction perpendicular to the yield surface. This can be attributed to the presence of true stresses (p) in the dissipation function (through the functions A and B in Eq. 8). It should be noted that plastic flow is associated in dissipative stress space (χ_p, χ_q) (Eq. 16). However, this feature is not transferred during the transition from dissipative stress space to true stress space, because of the criterion of maximizing the rate of dissipation. Note that, at the intersection point of the yield surface with the CSL, the plastic flow is perpendicular to the yield surface and its components are only in the q-axis direction. This shows that the model is compatible with Critical State theory, which implies that at the Critical State conditions, no plastic volumetric strains are produced due to the plastic flow direction being only in the direction of the q-axis.

One of the distinguishing features of a constitutive equation derived by thermodynamics principles, in comparison with other fully phenomenological models (e.g. hypoelasticity), is that they ensure the satisfaction of thermodynamics laws. This feature is illustrated by two examples. Assume that an elastic material follows the closed stress path (a)-(b)-(c)-(d)-(a) in triaxial stress space, as shown in
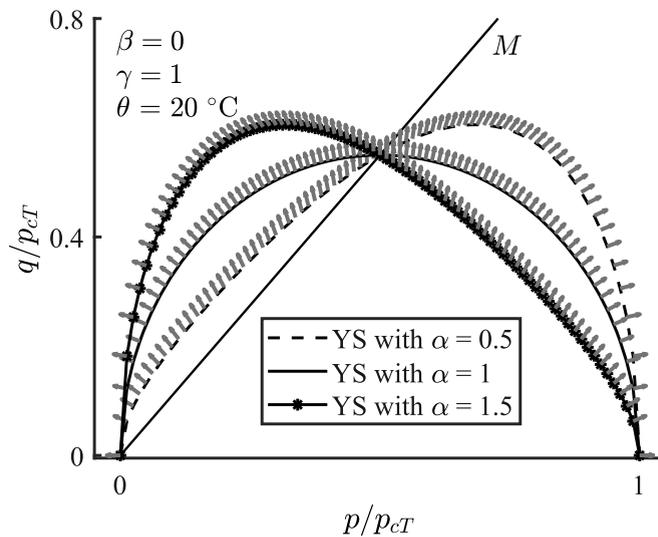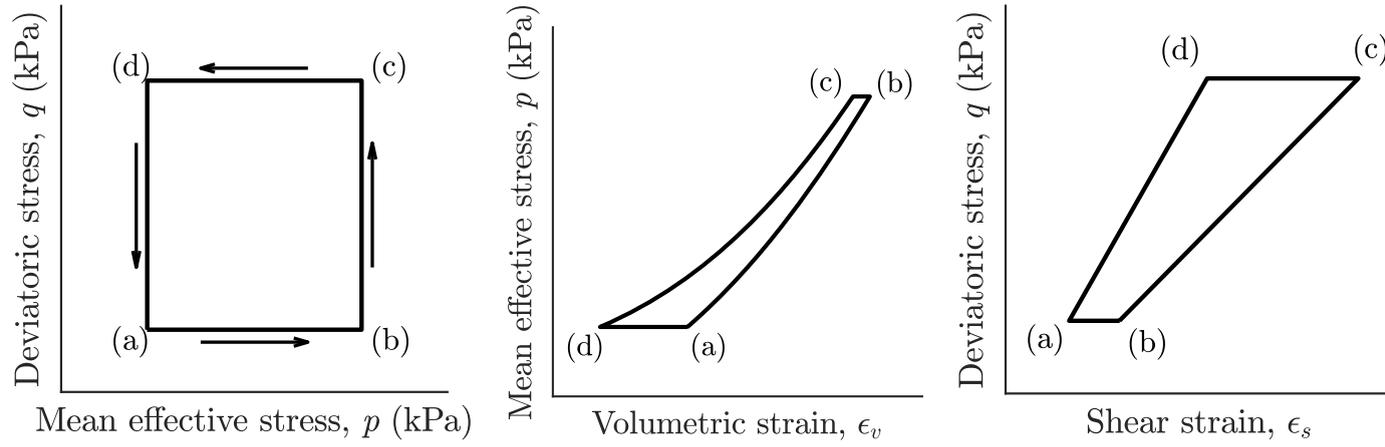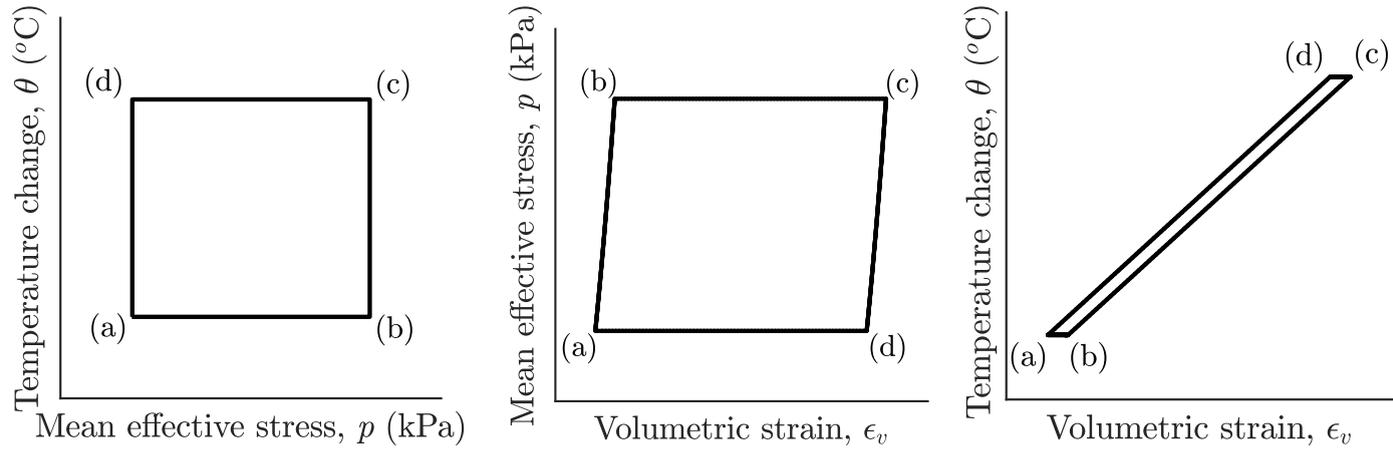

Fig. 4. Plastic flow direction for three different yield surfaces.

Fig. 5. (a) Mechanical loop in elastic stress space; (b) mean effective stress vs. volumetric strain; (c) deviatoric stress vs. deviatoric strain.

Fig. 6. (a) Temperature loop in temperature vs. mean effective stress space; (b) mean effective stress vs. volumetric strain; (c) temperature vs. volumetric strain.
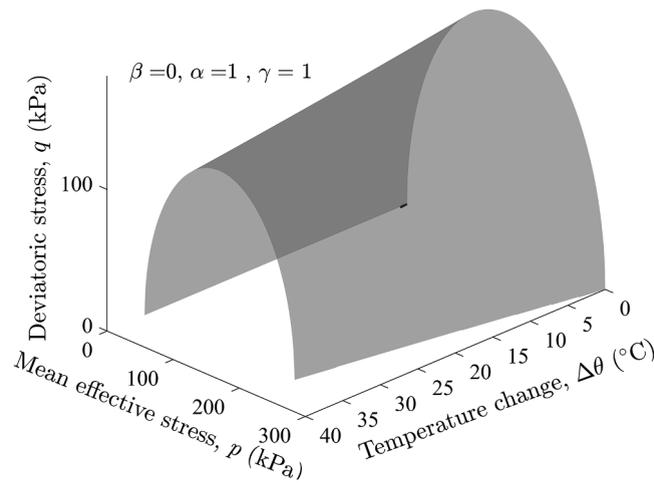
Fig. 7. The yield surface in three dimensional p-q-θ space.

Fig. 5(a), under isothermal conditions (constant temperature). This stress path is designed specifically to illustrate a reversible process, as the initial and end points of the loop coincide with each other. The material is firstly subjected to an increase in mean effective stress from point (a) to point (b), followed by an increase in deviatoric stress at constant p, up to point (c). Under constant deviatoric stress q from that point, the mean effective stress is reduced until point (d). In the final stage, the deviatoric stress is reduced in order that the stress state returns to its initial value at point (a). The corresponding mean effective stress versus volumetric strain and deviatoric stress versus deviatoric strain response for this stress path are depicted in Fig. 5(b) and Fig. 5(c), respectively.

The elastic properties of materials are in fact stress path independent, i.e., elasticity only depends on the final state of the material (Puzrin, 2012). Hence, since the initial and final stress states (point (a) on the stress path) are identical, the initial and final states of the strains (both elastic volumetric and deviatoric strains in Fig. 5(b) and Fig. 5(c)) should be identical. As illustrated in Fig. 5(b) and Fig. 5 (c), this is indeed the case. This behavior represents the conservation of energy (first law of thermodynamics) during a reversible process and the model is capable of capturing this behavior. On the other hand, non-linear fully phenomenological models (which are commonly used for soils) lack this principle, which may lead to strains which have no physical meaning. The hyperelasticity employed here overcomes this dilemma by using volumetric-deviatoric coupling terms. This means that volumetric behavior affects deviatoric behavior, as observed in geomaterials (Puzrin, 2012), and vice versa. However, these coupling terms are mostly ignored in models proposed for geomaterials, meaning that the volumetric and deviatoric behaviors are considered independent.

In the second example, an elastic material is subjected to stress and temperature variations, illustrated by the closed loop of points
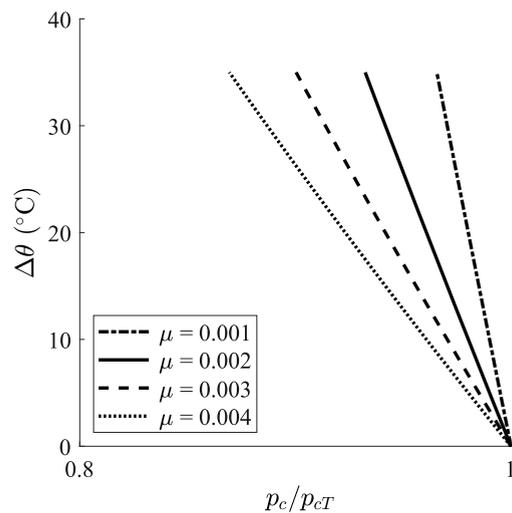

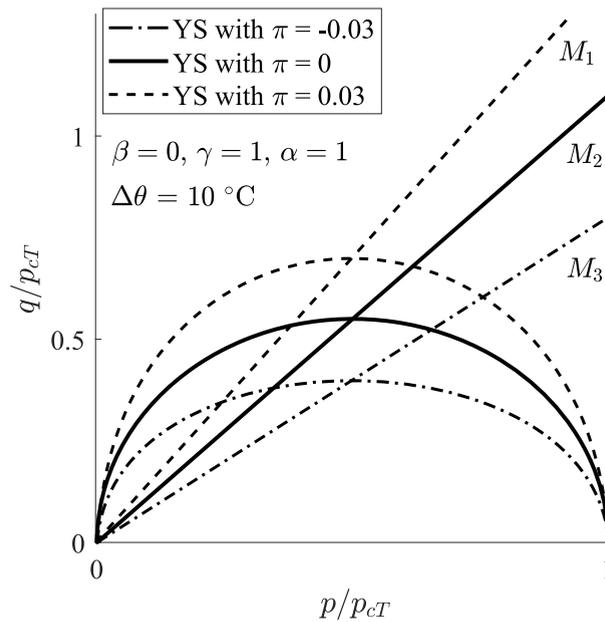**Fig. 8.** Effect of thermal softening parameter.

Fig. 9. Effect of parameter π on the shape and size of the yield surface.

(a)-(b)-(c)-(d)-(a) in Fig. 6(a). From the initial state of stress and temperature represented by point (a), the mean effective stress under constant temperature is increased until the material is at a new stress state at point (b). The material is then heated under constant p to reach point (c). At this temperature the mean effective stress is reduced (to point (d)) and finally the material is cooled down at constant p to its initial state at point (a). The corresponding volumetric strain variation with mean effective stress p and temperature θ is shown in Fig. 6(b) and Fig. 6(c), respectively.

The closed loop θ-p path represents a reversible process in which the behavior is thermo-elastic. As seen in Fig. 6(b) and Fig. 6(c), the material forms a closed loop for the corresponding p and θ versus volumetric strain, in that the initial and final states are identical. This proves the thermodynamical consistency of the model, which is important for thermo-mechanical models when simulating change in volume of soils subjected to temperature variation, since the volume variation of over-consolidated soils during heating is considered a thermo-elastic response (Hong, Pereira, Tang, & Cui, 2013). In literature, models exist in which the volumetric thermal expansion coefficient is related to the over-consolidation pressure or temperature (or both). Although this might appear satisfactory for predicting the behavior, the models are not necessarily thermodynamically consistent. As a result, elastic strains can be produced where energy is lost.

Table 3
Summary of model parameters.

| Parameters	Towhata *et al.* (1993)	Abuel-Naga *et al.* (2006, 2007b)	Uchaipichat & Khalili (2009)	Cekerevac & Laloui (2004)	Ghahremannejad (2003)	Graham, Tanaka, Crilly, & Alfaro (2001); Tanaka *et al.* (1997)
α (-)	0.2	0.9	0.75	0.6	1.3	0.7
γ (-)	0.9	0.4	1.1	1.05	0.94	0.72
λ (-)	0.24	0.43	0.090	0.13	0.15	0.087
κ (-)	0.05	0.09	0.006	0.028	0.03	0.017
M_0 (-)	0.75	0.8	1.218	0.82	0.85	1.07
$\overline{K}$ (-)	38	17.5	75	500	34 (=$1/\kappa$)	59 (=$1/\kappa$)
$\overline{G}$ (-)	80	15	170	700	150	20
n (-)	1.0	0.7	0.95	0.35	1.0	1.0
m (-)	1.0	1.0	0.85	0.7	1.0	1.0
α^* (1/K)	-3.1 × 10^{-6}	-3.1 × 10^{-6}	-3.4 × 10^{-5}	-1.8 × 10^{-4}	-3 × 10^{-5}	-1.5 × 10^{-4}
μ (1/K)	5.95 × 10^{-3}	7.7 × 10^{-3}	3.4 × 10^{-3}	7.34 × 10^{-4}	9.09 × 10^{-4}	7 × 10^{-2}
π (1/K)	0	0	0	1.05 × 10^{-3}	-1.6 × 10^{-3}	0
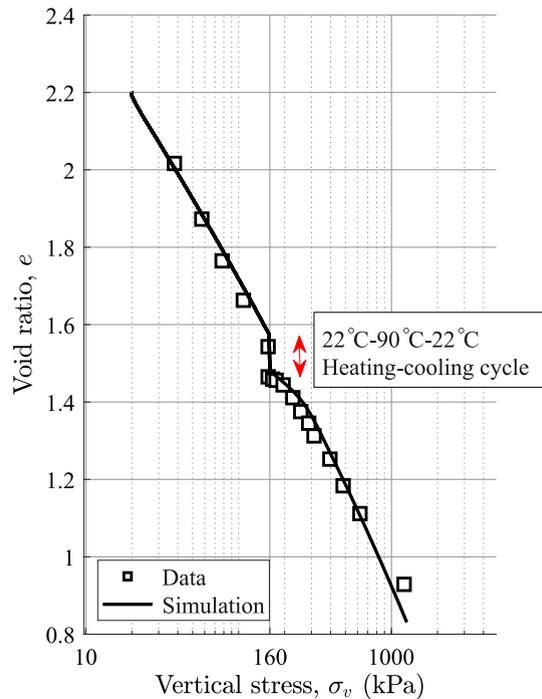
Fig. 10. Comparison of void ratio vs. vertical stress predicted by model with experimental data of Towhata *et al.* (1993).

5. Temperature effects

Fig. 7 shows the three-dimensional yield surface (Eq. 18) with respect to deviatoric stress q, mean effective stress p and temperature change $\Delta\theta°$C, along with the corresponding parameter values used for the illustration. The yield surface is bounded at an initial pre-consolidation pressure (p_{c0}) of 200 kPa at zero temperature change ($\Delta\theta=0°$C). As the temperature increases, the apparent pre-consolidation pressure (p_{cT}) decreases exponentially (according to Eq. 13) which leads to a smaller yield surface. As the yield surface shrinks the thermo-elastic domain (the area inside the yield surface) decreases. This means that for a material sheared in an over-consolidated and isotropic state (for example loading from $q=0$ at $p=100$ kPa in Fig. 7), the yielding stress state is reached, i.e., the yield surface is encountered, at lower stress states when the material is at higher temperatures.

The parameter that controls the bounded size of the yield surface when the temperature changes, i.e., controls the curvature of the apparent pre-consolidation variation, is μ in Eq. 13, which is called the thermal softening parameter. Eq. 13 can also be presented as $p_{cT}=p_c e^{-\mu(\theta-\theta_0)}$, where p_c is the pre-consolidation pressure at ambient temperature. By normalizing the equation by p_c, the variation of μ due to change in temperature can be determined ($p_{cT}/p_c=e^{-\mu(\theta-\theta_0)}$). This variation for four different values is illustrated in Fig. 8. As the value of μ increases, the yield surface shrinks faster in comparison with lower values when subjected to temperature increase. Note that this parameter is material specific and thus, depending on the soil type, the apparent pre-consolidation pressure can reduce dramatically (higher values of thermal softening parameter) or slightly as the temperature increases.

Depending on the constituents of the soil, the Critical State stress ratio M may increase or decrease as the temperature changes (Eq. 12). This change is considered through the parameter π in Eq. 12 and its effect on the yield surface is presented in Fig. 9. In this figure, the axes of deviatoric stress q and mean effective stress p are both normalized by the apparent pre-consolidation pressure p_{cT} to eliminate the thermal softening mechanism on the surface. Both positive and negative values can be assigned to π. Positive values of π result in a stretch in the minor axis (along the q-axis), i.e., an increase in size of the yield surface, while negative values cause a reduction in size.

In summary, the effect of temperature on the shear and volumetric behavior of soils is incorporated by the addition of thermo-elasticity into the energy potential (Eq. 2), a thermal softening mechanism (Eq. 13), and a Critical State stress ratio variation with temperature (Eq. 12) into the dissipation function (Eq. 8). Because all the constitutive equations are derived based on these two potentials, thermal effects are embedded into all the governing equations, including those for elasticity (Eq. E-5), plastic flow (Eq. 19),
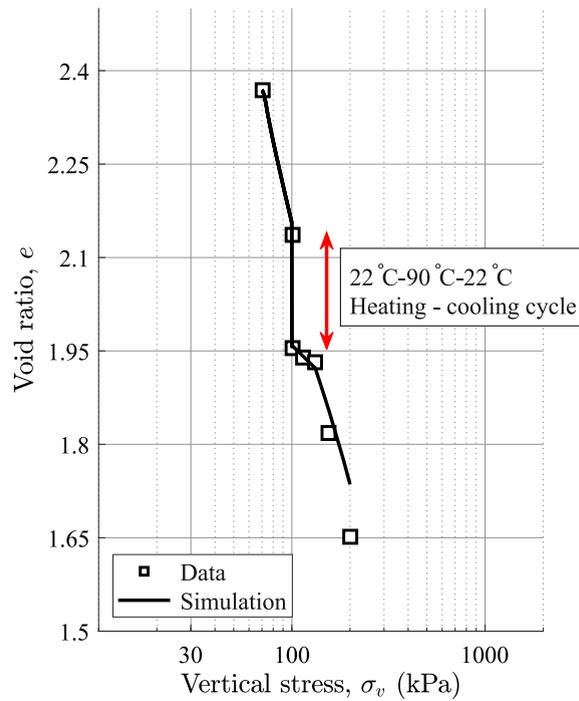
(a)
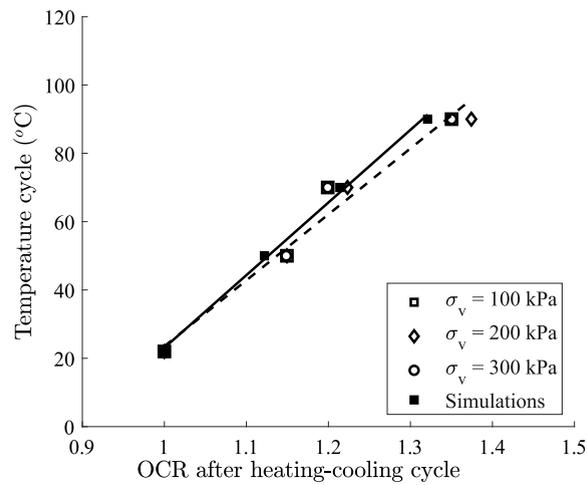
(b)

Fig. 11. Comparison of model predictions with experimental data of Abuel-Naga *et al.* (2007b): (a) void ratio vs. vertical stress; (b) attained OCR after thermal cycle vs. amplitude of the thermal cycle.
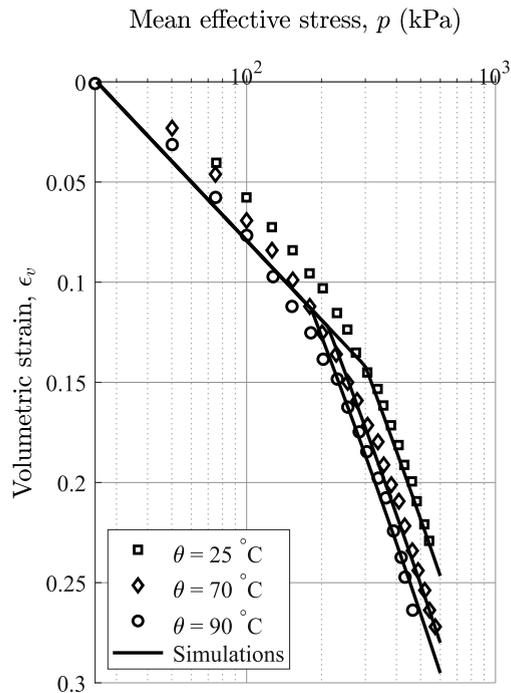
Fig. 12. Comparison of model predictions of volumetric strain vs. mean effective stress, during isotropic compression at different temperatures, with experimental data of Abuel-Naga *et al.* (2006).

plastic strain magnitude (plastic multiplier) (Eq. 22 or Eq. E-8), and the hardening rule (Eq. 20), which implies that thermal effects are coupled with the mechanical behavior of soils.

6. Model performance

The performance of the model is validated by comparing simulations with a wide range of experimental data from oedometer and triaxial tests under drained and undrained conditions on different soil types. The tests cover a wide variety of stress paths and loading histories. The calibrated parameters used for the simulations are reported in Table 3.

Towhata et al. (1993) test

Towhata *et al.* (1993) performed an oedometer test on a kaolinite clay and the void ratio variation with vertical stress is shown in Fig. 10. First, the specimen was subjected to a vertical stress increase from 20 kPa to 160 kPa at a room temperature of 22°C. Next, with the vertical stress held constant at 160 kPa, the specimen was heated to 90°C and then cooled back to room temperature (22°C). This was followed by further compression with the vertical stress increasing to 1260 kPa at room temperature. During the heating-cooling cycle (22°C-90°C-22°C), the soil attained a denser state (observed via a void ratio reduction seen in Fig. 10). As a result of the compression, the pre-consolidation pressure increased and the stress state of the soil changed from a normally-consolidated state to a slightly over-consolidated state. This is demonstrated by the bilinear response of the soil during the re-compression. On re-compressing the soil, starting from the vertical stress of 160 kPa, the initially stiffer response of the soil was due to elasticity and was therefore reversible. After reaching the new pre-consolidation pressure, irreversible behavior was observed, as the response followed the normally consolidated line (for the ambient temperature).

The numerical simulation in Fig. 10 captures the void ratio reduction during the thermal cycle, due to the thermal shrinkage mechanism of the elastic domain by Eq. 13. During heating, the apparent pre-consolidation tends to decrease due to the thermal softening mechanism. However, plastic volumetric strains are simultaneously produced which triggers the hardening mechanism. These two mechanisms compensate for each other, resulting in an unchanged apparent pre-consolidation pressure (at 90°C). During cooling, the apparent pre-consolidation pressure increases (hardening due to cooling, without any production of plastic volumetric strain) and the yield surface expands, resulting in the current stress state (vertical stress of 160 kPa) to be located inside the yield surface. Thus, further compression gives an elastic response, followed by an elasto-plastic response when the stress state reaches the yield surface. In conclusion, the model successfully captures the impact of a thermal cycle hardening mechanism exhibited by fine-

(a)

(b)

(c)
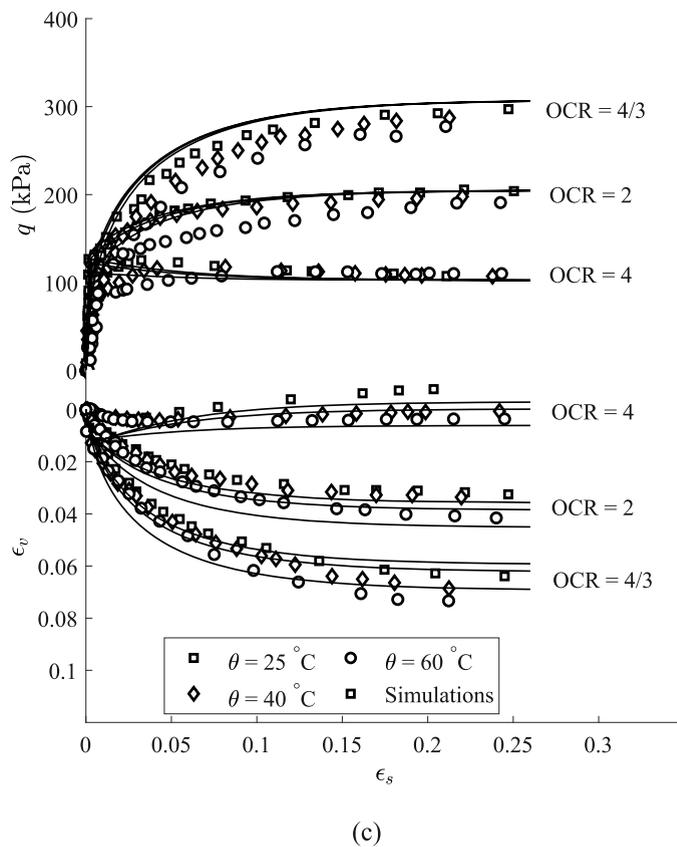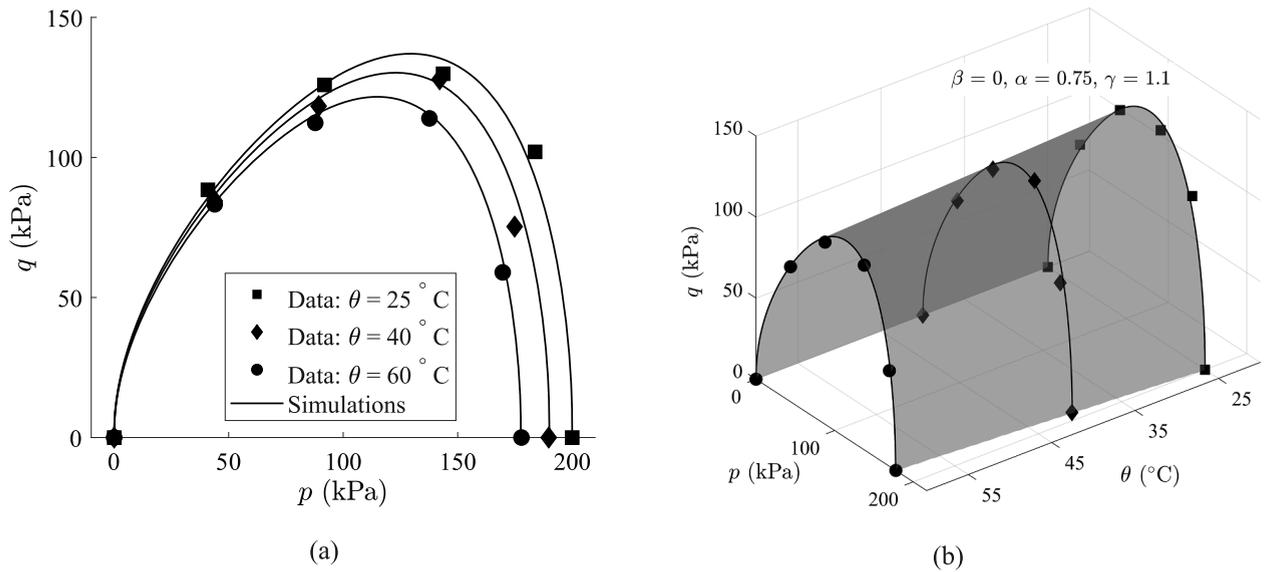
Fig. 13. Comparison of model predictions with experimental data of Uchaipichat & Khalili (2009): (a) yield surfaces at different temperatures in *p-q* stress space; (b) yield surfaces at different temperatures in three dimensional *p-q-θ* space; (c) deviatoric stress and volumetric strain vs. deviatoric strain at different OCRs.

grained soils.

Abuel-Naga et al. (2007b, 2006) tests

Oedometer and triaxial compression tests on Bangkok clay, performed by Abuel-Naga *et al.* (2007b, 2006), are presented in Fig. 11 and Fig. 12, respectively.

(a)

(b)
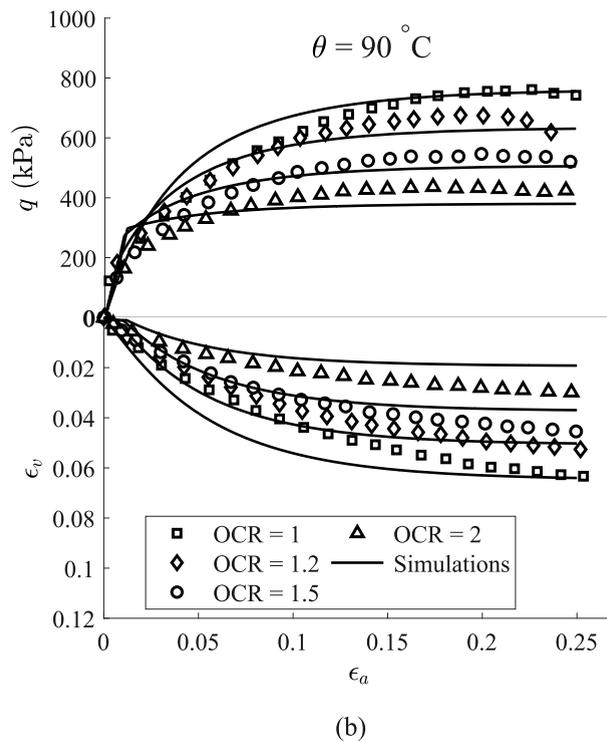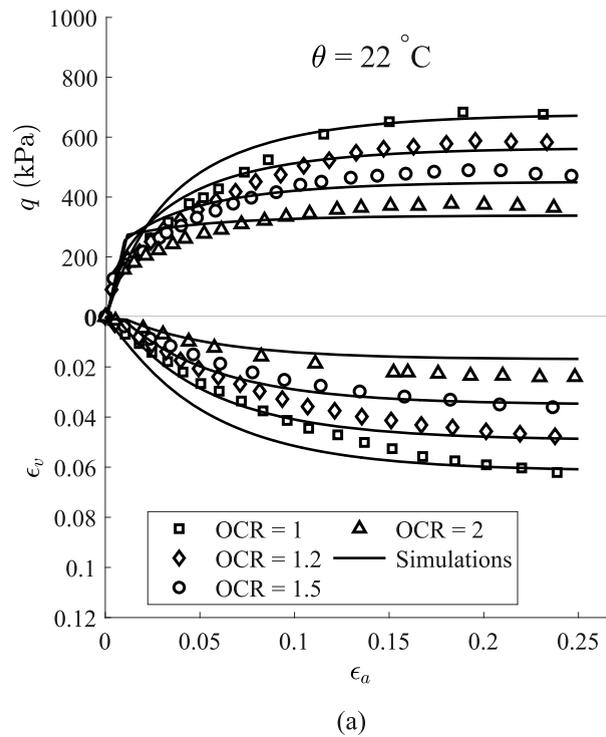
Fig. 14. Comparison of model predictions of deviatoric stress and volumetric strain vs. axial strain at different OCRs with experimental data of Cekerevac & Laloui (2004): (a) at θ=22°C; (b) at θ=90°C.

In Fig.11(a), the void ratio variation with vertical stress for Bangkok clay, following a testing procedure similar to Towhata *et al.* (1993), is presented. When the soil was subjected to a thermal cycle at a vertical stress of 100 kPa, the void ratio reduced (mostly due to permanent volumetric deformation). Again, the model results closely match the experimental results. As explained previously, this
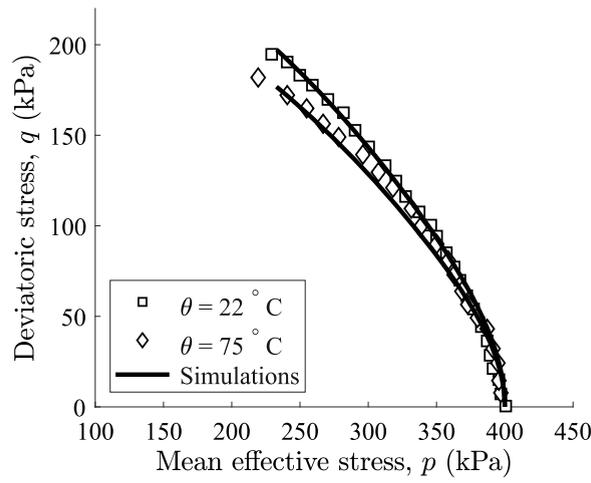
(a)
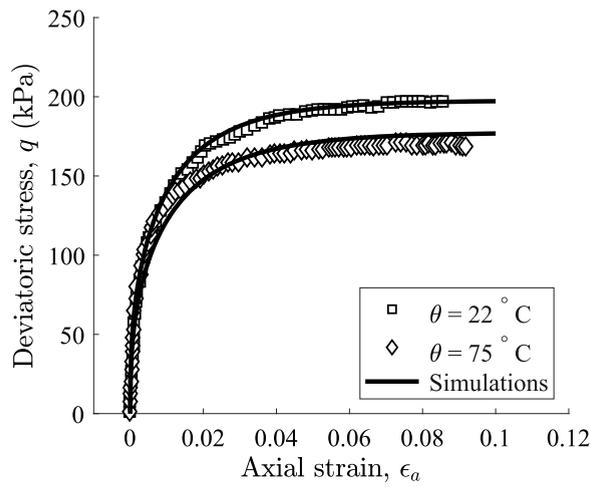
(b)
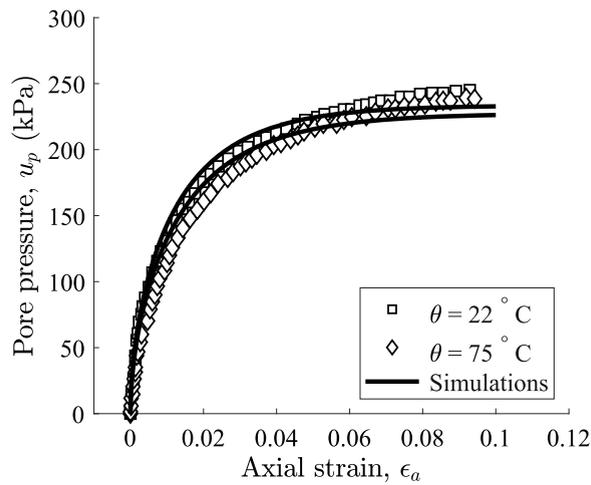
(c)

Fig. 15. Comparison of model predictions with undrained experimental data of Ghahremannejad (2003) at different temperatures: (a) stress path; (b) deviatoric stress vs. axial strain; (c) pore pressure vs. axial strain.
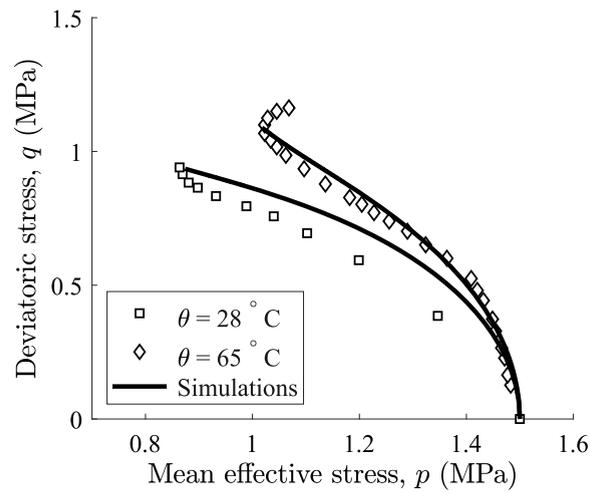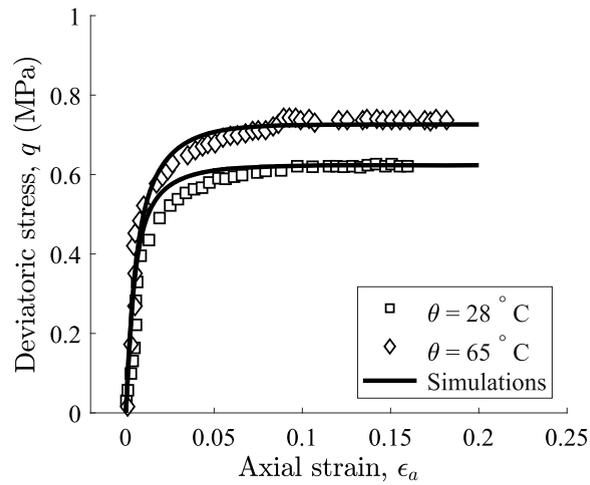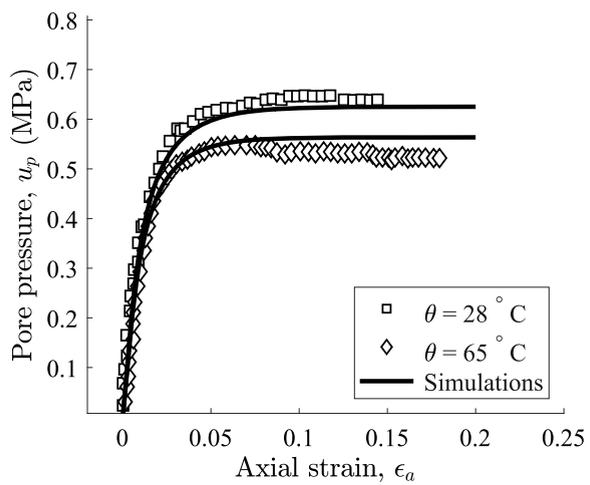
Fig. 16. Comparison of model predictions with undrained experimental data of Graham *et al.* (2001) and Tanaka *et al.* (1997) at different temperatures: (a) stress paths; (b) deviatoric stress vs. axial strain; (c) pore pressure vs. axial strain.

reduction of void ratio results in a slightly over-consolidated stress state. Abuel-Naga et al. (2007b) repeated the testing procedure for different vertical stresses (100, 200 and 300 kPa) and for a wide range of heating-cooling cycle magnitudes. The reported over-consolidated stress states attained after thermal cycles with respect to the thermal cycle amplitude are shown in Fig. 11(b). As expected, the larger the magnitude of the thermal cycle, the greater the over-consolidated state achieved, which implies a larger decrease in void ratio during the thermal cycle. The computed results are compared with the experimental data in Fig. 11(b), showing that the model is capable of capturing the heating-cooling hardening behavior of soils. An interesting point that can be inferred from the experimental data is that the OCR values attained after each heating-cooling cycle are independent of the stress state (the vertical stress at which the thermal cycle is applied), and this has also been well captured by the model.

Fig. 12 shows the volumetric behavior of the same soil in an isotropic compression test with triaxial apparatus, at three different temperatures of 25, 70 and 90°C. At room temperature (25°C), samples were first isotropically compressed to a mean effective stress of 300 kPa and then unloaded to 25 kPa to attain an OCR of 12. Under drained conditions, the samples were then heated to the target temperature, followed by an isotropic re-compression to beyond 300 kPa. The model simulations are compared with the experimental data in Fig. 12. Since the soil is initially highly over-consolidated, the initial response is elastic compression. For the sample at a temperature of 25°C, the response becomes elasto-plastic at a stress state of 300 kPa. For samples compressed at elevated temperatures, the elasto-plastic response is triggered at mean effective stresses lower than 300 kPa, due to the shrinkage of the yield surface due to the increase in temperature. The predictions of the model for all temperatures are satisfactory and capture well the difference in yield stress due to temperature difference.

Uchaipichat & Khalili (2009) tests

In Uchaipichat & Khalili (2009), the shear behavior of a fully saturated silty soil under drained conditions was investigated at three temperatures (25, 40 and 60°C) and for three mean effective stresses (50, 100 and 150 kPa). Prior to shearing, all the samples were isotropically loaded to 200 kPa and unloaded to 50 kPa under isothermal conditions (constant temperature of 25°C). Hence, all samples had an initial pre-consolidation pressure of 200 kPa. The samples were then heated to the desired temperatures (25, 40 and 60°C) and sheared under drained conditions until failure. The experimental data and model predictions are presented in Fig. 13. Fig. 13 (a) and Fig. 13(b) show the yield surface at different soil temperatures, starting with the initial surface corresponding to a pre-consolidation of 200 kPa at 25°C, in p-q stress space and p-q-θ space, respectively. From the laboratory data, it is obvious that, as the temperature increases, the yield surface shrinks in size and the pre-consolidation pressure decreases. The proposed model is capable of capturing both the shape of the yield surface and the yield surface shrinkage.

In Fig. 13(c), the shear stress versus shear strain and volumetric strain versus shear strain curves are shown. The predictions of the model are in good agreement with the experimental data for different over-consolidated states sheared at mean effective stresses of 150, 100 and 50 kPa. Changes in the Critical State stress ratio (M) have not been reported and the shear strengths of all samples sheared at identical mean effective stress reach the same ultimate value (Critical State), regardless of temperature effects. Therefore, π=0 and the simulations are in agreement with the experimental data.

Cekerevac & Laloui (2004) tests

Cekerevac & Laloui (2004) investigated the thermo-mechanical behavior of a re-constituted kaolin clay under drained conditions. The samples at ambient temperature (22°C) were initially isotropically consolidated to 600 kPa and then unloaded to reach the desired over-consolidation ratio (1, 1.2, 1.5 and 2). Under drained conditions, the samples were heated to reach the desired temperatures (22 and 90°C). When the samples were equilibrated at the target temperatures, they were sheared until failure. The model predictions for the two temperatures are compared with the experimental data in Fig. 14. The model predicts the deviatoric stresses and volumetric strains of the soil with reasonable accuracy. It is worth noting that the Critical State stress ratio had increased from 0.82 at 22°C to 0.89 at 90°C, which resulted in a higher ultimate shear stress (at the Critical State) at the elevated temperature in comparison with the ultimate shear stress at the ambient temperature, which is well captured by the model results.

Ghahremannejad (2003) tests

Ghahremannejad (2003) conducted a series of drained and undrained triaxial tests with different mechanical loading and heating stages on normally consolidated illitic clay. From those tests, two undrained tests were selected for testing the model. In these experiments, in contrast to Uchaipichat & Khalili (2009) and Cekerevac & Laloui (2004), the soil was first heated to the desired temperature, and then isotropically compressed (to a mean effective stress of 400 kPa). With the temperature then kept constant, the specimens were sheared under undrained conditions. The test results for temperatures of 22°C and 75°C, along with the predictions of the model, are shown in Fig. 15. Fig. 15(a), Fig. 15(b) and Fig. 15(c), respectively, show the undrained stress path in p-q stress space, and the corresponding deviatoric stress and pore pressure versus deviatoric strain responses. The soil at a temperature of 75°C shows a softer behavior than the soil at a temperature of 22°C, and its shear strength is lower at Critical State conditions. In other words, the Critical State stress ratio is decreased at elevated temperatures.

Comparison of the simulations with the experimental data (Fig. 15) indicates that the current model successfully captures the softening behavior of the soil at elevated temperatures, due to the temperature-dependent Critical State stress ratio controlled through the parameter π (Eq. 12). Since the soil at the elevated temperature (75°C) was heated before being isotropically compressed, the thermal softening mechanism in Eq. 13 becomes deactivated (because $\theta = \theta_0$). Hence, the yield surface for any temperature (in this case, 22°C and 75°C) only expands isotropically due to compression and is bounded at 400 kPa. However, the size of the yield surface at θ =75°C is smaller than the size of the yield surface at θ =22°C due to the reduction of M at higher temperatures. As a result, the model predicts a softer response at elevated temperatures.

Graham et al. (2001) and *Tanaka et al. (1997)* tests

The undrained thermo-mechanical behavior of a normally consolidated illitic clay was addressed in the work of Graham et al. (2001) and Tanaka et al. (1997). The experimental results, including stress paths, shear stress evolution and pore water pressure
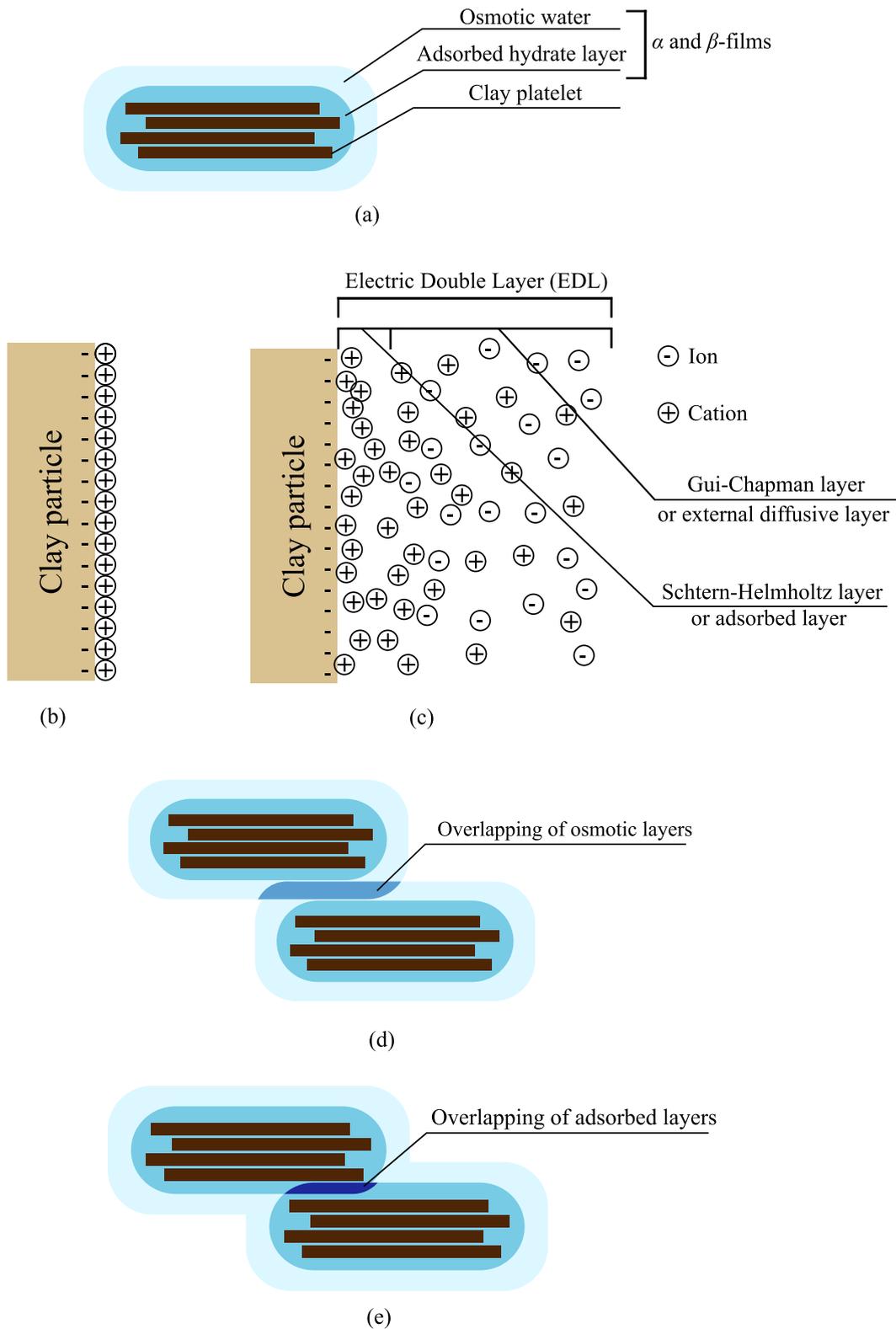
Fig. 17. After Osipov (2015): (a) clay particle with different hydrate layers; (b) electric field of clay particle in dry condition; (c) electric field of clay particle in wet condition; (d) development of disjoining pressure during overlapping of osmotic layers; (e) development of disjoining pressure during overlapping of adsorbed layers.

changes during undrained shearing at two different temperatures, are shown in Fig. 16. Prior to undrained shearing, the samples were isotropically consolidated to 1.5 MPa at room temperature (28°C) and subsequently heated to reach the desired temperatures (28 and 65°C). Due to the drained heating process, the samples attained different void ratios (due to the hardening mechanism) before the undrained shearing stage. The soil did not show any increase in the Critical State stress ratio (i.e. $\pi=0$). The predictions of the model show good agreement with the laboratory data.

7. Discussion: Micro-mechanics, internal stresses, and physicochemical processes during heating/cooling

The thermo-chemo-hydro-mechanical behavior of soils, especially fine-grained soils, is governed by the size of the particles and pore spaces between them, ranging from nano-metres to micro-metres. Thus, understanding the characterization of fine grained soils in a continuous manner, scaling from nano- to micro-metres, is important to inform material models. Experimental techniques, such as neutron diffraction and nano-XCT, provide information about physicochemical processes occurring in such a scaling range. To implement such knowledge in a continuum scale constitutive model, an up-scaling approach is required. However, up-scaling methods are challenging and mostly not straightforward, in part due to identifying appropriate length scales that satisfactorily represent the physics of deformation of the material. Lack of identifying suitable length scales leads to loss of information when up-scaling is applied.

The impact of temperature in the energy and dissipation functions presented in this model is based upon phenomenological considerations in a thermodynamically consistent continuum approach. The step-by-step approach in the derivation is conducive to an approach also considering micro-structural aspects, as has been undertaken in other constitutive approaches (e.g. Özdemir, Brekel-mans, & Geers, 2008). However, those approaches do not explicitly ensure the conservation of energy. This section attempts to qualitatively explain the processes that may occur during thermal loadings, in part to rationalize the choices made and, in part, as a first step towards a micro-mechanical model that is also consistent with thermodynamics principles.

Two main mechanisms have been proposed to understand some thermally-induced effects (Coccia & McCartney, 2012; Vega & McCartney, 2015):

1. Difference in thermal volumetric expansion coefficients between soil particles and water: During heating of a saturated soil, because of the differences in thermal expansion coefficient between soil particles and water (the thermal expansion coefficient of water, depending on the mineralogy of the soil, is 8–15 times higher than that of soil particles), excess pore water pressure is generated. If drainage is allowed, consolidation occurs which can lead to permanent volume change (if the sample is confined and not heavily over-consolidated). However, if drainage is not allowed (undrained condition), there is no consolidation and thus the pore water pressure is retained.
2. Change in the viscosity of water: The second mechanism is attributed to the change (decrease) in the viscosity of water during heating and the thermal creep of soil particles. Reduction of the water viscosity results in easing of water flow through the void space. As the flow increases, consolidation increases which can eventually lead to plastic deformation.

Note that neither of the aforementioned mechanisms can explain the changes in shear or yielding behavior. Various phenomena are described in the literature, where one of the major features which govern the mechanical behavior of fine-grained soils, that is the internal forces, have been ignored. Therefore, further investigation is required to understand the actual mechanisms occurring in the soil.

The surface areas of fine-grained soils (like clays), in a specific mass of soil, are higher than for coarse-grained soils like sands (Mitchell & Soga, 2005). These surfaces are mostly negatively-charged, which causes water molecules and cations to be adsorbed on the surface of the grain (Mitchell & Soga, 2005; Osipov, 2015; Sedighi & Thomas, 2014). As a result, internal forces in the presence of external forces act between soil particles (Osipov, 2015) and are called "*physicochemical internal forces*". These forces develop inside the soil mass and, depending on the source of the forces, may increase or decrease the internal energy of the soil. The major processes occurring inside the soil mass, which lead to the production of physicochemical forces, can be summarized as (Osipov, 2015):

1. Development of an electric double layer (EDL) and an electrostatic field of particles
2. Occurrence of osmotic process
3. Formation of thin water layers on soil particles (hydrate layers)
4. Capillary menisci in unsaturated soils
5. Concentration of ions in the liquid

and are shown schematically in Fig. 17. In saturated soils (which are considered here), the effect of capillary menisci can be ignored. The stability of the soil mass is directly controlled by the balance between the attractive and repulsive forces generated during physicochemical processes. Attraction forces are due to Van der Waals forces between soil particles, whereas the repulsive forces are due to electrostatic interaction, due to the overlapping EDLs of particles and formation of adsorbed water films on the mineral surface of particles with specific structure.

The thermodynamic equilibrium between physicochemical forces (attractive and repulsive forces) leads to the development of thin hydrate films on the surface of the particle (Fig. 17(a)), between any pair of particles in contact. Any change in the system, due to mechanical or thermal loads, disturbs the thermodynamic balance of the system and changes its energy level. As a result, the thickness of hydrate layers (Osipov, 2015) changes and additional pressures are produced in the interphase liquid layer. This excess pressure is called the "*disjoining pressure*" $\Pi_t(t)$ and arises to counteract the imposed changes (because of mechanical and thermal loads) by

keeping the soil-mass in equilibrium. The magnitude of the disjoining pressure is directly dependent on the thickness of the films, t, (i. e., on the level of overlapping of hydrate layers) and may attain positive or negative values (thickening or thinning of the layer, respectively). It should be noted that the strength and deformation properties of fine-grained soils are highly dependent on the disjoining pressure, resulting from physicochemical processes, of these hydrate films.

The total disjoining pressure due to different origins can be divided into three major independent sources which are additive (Deryaguin & Churaev, 1984):

$$\Pi_t(t) = \Pi_e + \Pi_m + \Pi_s \tag{23}$$

where Π_e, Π_m and Π_s are the respective electrostatic, molecular and structural components that act simultaneously with different governing laws.

Molecular forces (Van der Waals forces) are generated as the result of the molecular component of the disjoining pressure Π_m. These forces act as attractive forces at the surface of the soil particle, which result in thinning of the hydrate layer. The magnitude of this force depends on the surface area of the soil particles.

The surfaces of clay particles are negatively charged, which in dry conditions (Fig. 17(b)) are neutralized by cations adsorbed to the surface. In the presence of water (Fig. 17(c)), hydration weakens the interaction of the surface and the cations, and water molecules replace a portion of the cations on the clay surface; consequently, a portion of cations remain adjacent to the surface and form the so-called "*adsorption*" or "*Schtern-Helmholtz layer*", while other cations diffuse from the surface and develop the "*external diffusive layer of cations*" or the "*Gui-Chapman*" layer, also known as the osmotic hydrate layer. Thus, a double electric layer with positive-electric charge is formed, with the latter layer being thicker than the former layer (Osipov, 2015).

The diffusive layer provides a positive-electric field around the clay particles. In the case that the particles approach each other (due to mechanical loads), the positive-electric fields around the particles overlap (Fig. 17(d)), which increases the cation concentration and consequently the electrical potential. This increase of cation concentration produces local osmotic pressures that force water to flow between particles and attempt to separate (disjoin) them. This is how the electric component of the disjoining pressure, Π_e, arises and contributes as repulsive forces (Osipov, 2015).

The adsorption hydrate layer is strongly connected to the surface of the clay particles (the strength of adsorption depends on the mineralogy of the clay) and anisotropic stress states are formed inside it (Osipov, 2015). This anisotropic stress state and the adaption of water to the shape of the surface of the particle deforms the hydration bonds, which leads to a transformation of the structure of the water in the adsorbed film and imposes different properties compared to normal water. Increases in viscosity and the production of disjoining pressure are examples of different structural-mechanical properties of this hydrate layer (Churaev, Sobolev, & Zorin, 1971; Deryaguin & Churaev, 1984; Zorin, Sobolev, & Churaev, 1972). Again, when the clay particles approach each other in a way that the adsorbed hydrate layers of particles overlap (Fig. 17(e)), the layers start to be destroyed and the energy level increases, resulting in a thermodynamical imbalance. Consequently, disjoining pressure is developed to counteract the destruction of the hydrate layer and tends to separate particles. This repulsive pressure is called the structural-mechanical disjoining pressure Π_s (Deryaguin, 1986; Deryaguin & Churaev, 1984; Deryaguin, Churaev, & Muller, 1985; Israelachvili & Pashley, 1983) and overall, depending on the mineralogy and shape of the particles, forms anisotropic stress-states with different mechanical properties inside the hydrate layer.

According to the disjoining pressure isotherm (the relationship between the force developed as the result of the total disjoining pressure, Π_t, and the thickness of hydrate films, t), two stable water layers, namely α- and β-films, may form on clay particle surfaces (Deryaguin & Churaev, 1984). α-films are associated with thin layers with thicknesses around 10 nm, whereas β-films correspond to thick hydrate layers with thicknesses of nearly 100 nm.

The stability of β-films is dominated by electrostatic components of the disjoining pressure Π_e. Thus, they are highly sensitive to ion concentration surrounding the soil grains (in EDL and solvent) and show insensitivity to temperature variation (Deryaguin, 1986; Deryaguin & Churaev, 1972, 1984). On the other hand, α-films are mostly associated with the structural-mechanical component of the disjoining pressure Π_s. Therefore, the stability of these layers directly depends on the mineralogy and constituent properties of the clay particles and the hydrate layer. This hydrate layer shows a temperature-dependent behavior, as it thins when the temperature increases and disappears at temperatures close to 65°C (Deryaguin, 1986; Perevertaev & Metsik, 1966). Therefore, the impact of thermo-mechanisms on the mechanical behavior of soils can be determined from the behavior of this hydrate layer, when temperature varies. It should be noted that the β-films may break due to external mechanical loads. In this case, the disjoining pressure would develop only due to the overlapping of adsorbed layers and the structural component of the α-films governs its value.

The aforementioned physicochemical mechanisms may explain the thermo-mechanical behaviors observed in fine-grained soils. Soils with higher plasticity index PI have a higher level of chemical reactivity. Also, it has been observed that when the temperature is elevated, soils with a higher PI undergo higher thermally-induced volume changes compared to soils of a lower PI (demonstrated in Section 2). This may be attributed to α-films of different thicknesses, as, when the temperature of the soil mass increases, the α-film of soil particles with a higher PI becomes thinner. As a result, the water inside the hydrate layer squeezes out of the layer and elevates the pore pressure. Because of the volumetric reduction of soil grains due to thinning of the adsorbed hydrate layer (α-film) and excess pore water pressure generation, the (thermodynamically stable) state of the soil can be prone to moving to a thermodynamically unstable state. This means that during the transition from a thermodynamically stable condition to an unstable condition, the stress state of the soil becomes closer to the maximum stress state that the soil has attained during its heating-loading history. This implies that the state of the soil becomes closer to the yielding stress state. This behavior has been introduced in Eq. 13, as it calculates a smaller elastic domain when temperature increases, i.e., the stress state becomes closer to the yielding stress state and a micro-structural formulation could be included here. When a thermodynamically unstable condition is reached, as the result of the excess pore pressure generation

and volume reduction of soil particles (due to the thinning of hydrate layers), soil particles have a temporary freedom to rotate and reorient until they are positioned in a new thermodynamic equilibrium, with a higher contact area and a higher number of contacts with adjacent particles. This leads to an overall volume reduction, which has been observed when a soil is subjected to heating (as shown in Fig. 3).

At the same time, due to change in the thickness of the hydration layer, new anisotropic stress states are generated inside the film to counteract the instability caused by temperature variation and to stabilze the soil particles at a new thermodynamic equilibrium. Consequently, new hydration bonds are formed and new structural-mechanical properties occur. The modification in structural-mechanical properties leads to different yield values (observed in Fig. 1 and captured also by Eq. 13) and shear properties (variation of Critical State stress ratio with temperature, Fig. 2). Depending on the newly formed hydration bonds, the friction angle of soil particles may change (increase or decrease) or remain unchanged. This behavior is encapsulated in Eq. 12, and could be updated with a micro-structural formulation which well simulates the hardening and softening response of soils due to change in friction angle when temperature changes.

8. Conclusions

A constitutive model based on thermodynamics principles has been developed using the hyperplasticity framework. The formulation is based on a newly proposed Gibbs-type free energy and a newly proposed dissipation potential function in which different thermo-mechanisms have been embedded. The model explicitly incorporates thermo-elasticity, pre-consolidation pressure and Critical State stress ratio as a function of temperature, to capture the thermo-mechanical behavior of fine-grained soils. The model consists of 12 (or as few as 10 with some typical assumptions) parameters, which all have physical meaning and can be determined from conventional geotechnical laboratory tests. The model has been used to predict the thermo-mechanical behavior of fine-grained soils and is shown to capture the observed temperature effects.

Declaration of Competing Interest

The authors declare that they have no known competing financial interests or personal relationships that could have appeared to influence the work reported in this paper.

Acknowledgments

Appendix A. Thermodynamics of continua

This section explains the thermodynamics of continuum media and how the hyperplasticity framework uses the laws of thermodynamics to provide a platform for extracting the constitutive equations for different materials, including fine-grained soils. The formulations and notations in this section are in accordance with those in Collins & Houlsby (1997); Houlsby (2014); Houlsby & Puzrin (2000, 2002, 2007); Puzrin (2012). The platform described in this section is used to derive the constitutive equations in Section 3.

For a system in a state of thermodynamic equilibrium, all laws of thermodynamics apply. The first and second laws introduce two properties of the system. From the first law, the law of energy conservation, a property named "*internal energy*" is defined, in which the total power input to the system (e.g. work input $\dot{W} = \boldsymbol{\sigma} : \dot{\boldsymbol{\varepsilon}}$, and heat supply or net heat flux $\dot{Q} = q_{,k}$) is identical to the rate of change of the internal energy of the system (Houlsby & Puzrin, 2007):

$$\dot{u} = \boldsymbol{\sigma} : \dot{\boldsymbol{\varepsilon}} - q_{,k} \tag{A-1}$$

where $\boldsymbol{\sigma}, \dot{\boldsymbol{\varepsilon}}, \boldsymbol{q}$ and $q_{,k}$ are the stress and strain increment tensors, heat flux vector and its spatial derivative (a scalar value), respectively. The comma in the subscript indicates spatial differentiation with respect to the k direction and the symbol ":" is the double contraction operator.

The second law of thermodynamics states that a property of the system called entropy s exists, in which its rate is non-negative (Houlsby & Puzrin, 2007). This is best shown through the Clausius-Duhem inequality:

$$\dot{s} \geq -\left(\frac{\boldsymbol{q}}{\theta}\right)_{,k} \tag{A-2}$$

where $\boldsymbol{q}/\theta$ is the entropy flux vector and θ is the absolute temperature.

The above inequality can be rewritten as $\dot{s} + \left(\frac{\boldsymbol{q}}{\theta}\right)_{,k} = \dot{s} + \frac{q_{,k}}{\theta} - \frac{\boldsymbol{q} \cdot \boldsymbol{\theta}_{,k}}{\theta^2} = \frac{d^t}{\theta} \geq 0$, where d^t is the total dissipation and $\boldsymbol{\theta}_{,k}$ is the thermal gradient. Expanding this inequality and combining with the first law (Eq. A-1) (and eliminating the divergence of heat flux) results in:

$$\dot{u} = \boldsymbol{\sigma} : \dot{\boldsymbol{\varepsilon}} + \theta\dot{s} - \frac{\boldsymbol{q} : \boldsymbol{\theta}_{,k}}{\theta} - d^t \tag{A-3}$$

where $-\frac{q \cdot \theta_{,k}}{\theta}$ is the thermal dissipation and the rest of the dissipation $\left(d = d^t - \left(-\frac{q \cdot \theta_{,k}}{\theta}\right)\right)$ is due to mechanical deformation (mechanical dissipation). It is logical to consider the thermal and mechanical dissipation processes independently. Since the heat flux q and thermal gradient $\theta_{,k}$ have opposite signs, the thermal dissipation quantity is always positive and already satisfies the second law of thermodynamics (Houlsby & Puzrin, 2007). Hence, it can be excluded from the second law inequality which then requires the mechanical dissipation to be non-negative. Thus, the first and second laws of thermodynamics can be rewritten as:

First law:

$$\dot{u} + d = \boldsymbol{\sigma} : \dot{\boldsymbol{\varepsilon}} + \theta \dot{s} \tag{A-4}$$

Second law:

$$\theta \dot{s} + q_{,k} = d \geq 0 \tag{A-5}$$

A.1. Energy functions of dissipative materials

Soils and geomaterials in general can be categorized as dissipative materials, in that they undergo irreversible processes and part of their mechanical deformation transforms to heat. In conventional thermodynamics, the internal energy is defined by a set of visible and measureable kinematic (strain-like) variables, such as the strain tensor $\boldsymbol{\varepsilon}$, as well as entropy s and internal variable $\boldsymbol{\alpha}_i$ tensors (Houlsby & Puzrin, 2007; Puzrin, 2012). The essence of internal variables is essential to study the behavior of dissipative materials and they encapsulate the history of the material behavior due to irreversible processes (Houlsby & Puzrin, 2007).

The mechanical behavior and properties of soils, e.g. bulk and shear modulus, are most conveniently characterized by stress rather than strain (Einav & Puzrin, 2004; Houlsby, Amorosi, & Rojas, 2005). Therefore, it is convenient to define a form of energy function defined by independent variables of (effective) stress $\boldsymbol{\sigma}$ (from here on, all the stresses are effective), absolute temperature θ and internal variables $\boldsymbol{\alpha}_i$. Such an energy function is the Gibbs free energy, $g = g(\boldsymbol{\sigma}, \theta, \boldsymbol{\alpha}_i)$. Invoking the Legendre transform (explained in Appendix B) twice on the internal energy u, to interchange the role of strain $\boldsymbol{\varepsilon}$ with its work-conjugate stress $\boldsymbol{\sigma}$ and entropy s with absolute temperature θ, the first law of thermodynamics (Eq. A-4) is revised in terms of state variables for the Gibbs free energy:

$$\dot{g} + d = -\left(\dot{\theta} s + \dot{\boldsymbol{\sigma}} : \boldsymbol{\varepsilon}\right) \tag{A-6}$$

while the second law (Eq. A-5) remains unchanged.

Equating the rate (derivative with respect to time) of $g = g(\boldsymbol{\sigma}, \theta, \boldsymbol{\alpha}_i)$ with Eq. A-6 results in $\left(-\boldsymbol{\varepsilon} - \frac{\partial g}{\partial \boldsymbol{\sigma}}\right) : \dot{\boldsymbol{\sigma}} + \left(-s - \frac{\partial g}{\partial \theta}\right) \dot{\theta} + \left(-d - \frac{\partial g}{\partial \boldsymbol{\alpha}_i} : \dot{\boldsymbol{\alpha}}_i\right) = 0$. By assuming that the state variables of the energy function ($\boldsymbol{\sigma}$ and θ) vary independently, it can be deduced that:

$$\boldsymbol{\varepsilon} = -\frac{\partial g}{\partial \boldsymbol{\sigma}}, s = -\frac{\partial g}{\partial \theta}, -\frac{\partial g}{\partial \boldsymbol{\alpha}_i} : \dot{\boldsymbol{\alpha}}_i = d \geq 0 \tag{A-7}$$

By defining $-\frac{\partial g}{\partial \boldsymbol{\alpha}_i}$ as the "*generalized stress (tensor)* $\overline{\boldsymbol{\chi}}$" (Houlsby & Puzrin, 2007), the dissipation can be rewritten as:

$$d = \overline{\boldsymbol{\chi}} : \dot{\boldsymbol{\alpha}}_i = \left\langle \overline{\boldsymbol{\chi}}, \dot{\boldsymbol{\alpha}}_i \right\rangle \geq 0 \tag{A-8}$$

where $\langle \rangle$ is the inner product operator.

Three important conclusions can be derived from this equation:

1. The presence of internal variables (e.g. $\boldsymbol{\alpha}_i$) in the energy functions is necessary for dissipative materials; otherwise the term $\partial g / \partial \boldsymbol{\alpha}_i$ would be zero which results in zero dissipation and reversible behavior, similar to the observed behavior of elastic materials.
2. The dissipation should be a function of the rate of change of internal variables ($\dot{\boldsymbol{\alpha}}_i$); i.e., it is enough and sufficient to define the dissipation function only by the rate of change of internal variables ($d = d(\dot{\boldsymbol{\alpha}}_i)$) (Houlsby & Puzrin, 2007).
3. The dissipation function is the multiplication (inner product) of the derivative of the energy function with respect to the internal variable ($\partial g/\partial \boldsymbol{\alpha}_i$) and its corresponding rate of change ($\dot{\boldsymbol{\alpha}}_i$). This is similar to the properties of homogeneous functions (Appendix C).

In summary, the dissipation function should be homogeneous, non-negative and a function of the rate of internal variables.

A.2. Dissipation functions

The dissipation function of dissipative materials in general can be defined by "*generalized dissipative velocities $\boldsymbol{\nu}$*", state variables $\mathbf{x}$, e. g. stress (or strain), and temperature θ: $d = d(\mathbf{x}, \boldsymbol{\nu}, \theta) \geq 0$ (Houlsby, 2014). Note that $\boldsymbol{\nu}$ and $\mathbf{x}$ can be either scalar or tensorial. Generalized dissipative velocities is a term that covers both the rate of change of internal variables (e.g. rate of plastic strains, $\dot{\boldsymbol{\alpha}}_i$) and fluxes of various quantities (e.g. electrical charge). It can be proved that any thermodynamic function that is extensive (i.e. dependent

on the size of the system) is a homogeneous function (Addison, 1991). In addition, the dependence of the dissipation function on the generalized dissipative velocities is enough to define the non-negative dissipation function ($d = d(\boldsymbol{\nu})$). By considering these points and the fact that the dissipation function is a homogeneous function, by writing Euler's theorem (Eq. C-2) for the dissipation function d it can be concluded that:

$$n_h d = \frac{\partial d}{\partial \boldsymbol{\nu}} : \boldsymbol{\nu} \tag{A-9}$$

where n_h is the order of homogeneity of the function (see Appendix C).

A.3. Hyperplasticity approach

In hyperplasticity, the constitutive equations can be deduced by defining only the energy and dissipation functions, without the need to add additional assumptions (Houlsby & Puzrin, 2007). The thermodynamic work-conjugate of generalized velocities $\boldsymbol{\nu}$ is called "*generalized dissipative forces $\boldsymbol{\chi}$*" (which, depending on $\boldsymbol{\nu}$, can be a scalar or a tensor). These work-conjugates are critical because the relationship between them and the generalized dissipative velocities determines the constitutive equations governing the behavior of the material (Houlsby, 2014). It is assumed that the dissipation is a linear function of the generalized dissipative velocities $\boldsymbol{\nu}$, defined as $d = \boldsymbol{\chi} : \boldsymbol{\nu} = \langle \boldsymbol{\nu}, \boldsymbol{\chi} \rangle$, similar to Eq. A-8. By comparing with Eq. A-8 (since $\dot{\alpha}_i = \boldsymbol{\nu}$), the following result can be achieved:

$$\overline{\boldsymbol{\chi}} = \boldsymbol{\chi} \tag{A-10}$$

This is a key element in hyperplasticity and is often called Ziegler's orthogonality condition, although it has been noted by Rajagopal & Srinivasa (2019) that orthogonality is not a general requirement and must be linked to the physical process occurring.

To determine the generalized dissipative forces $\boldsymbol{\chi}$, Ziegler (1977) postulated that the direction of $\partial d / \partial \boldsymbol{\nu}$ produces maximal entropy (or maximal dissipation rate). From the geometry point of view, this direction is normal to the dissipation. From the mathematical point of view, the generalized dissipative forces can then be determined as:

$$\boldsymbol{\chi} = Y \frac{\partial d}{\partial \boldsymbol{\nu}} \tag{A-11}$$

where Y is a scalar that represents the magnitude of the generalized dissipative forces. Substituting Eq. A-11 into $d = \langle \boldsymbol{\nu}, \boldsymbol{\chi} \rangle$ results in:

$$d = Y \left\langle \boldsymbol{\nu}, \frac{\partial d}{\partial \boldsymbol{\nu}} \right\rangle \tag{A-12}$$

By comparing the dissipation functions in Eqs. A-9 and A-12, it can be concluded that $Y = 1/n_h$. Thus, the assumed dissipation function in the form of $d = \langle \boldsymbol{\nu}, \boldsymbol{\chi} \rangle$ is a homogeneous function of order n_h which is non-negative, which satisfies all the requirements of a dissipation function. The generalized dissipative forces are then determined as:

$$\boldsymbol{\chi} = Y \frac{\partial d}{\partial \boldsymbol{\nu}} = \frac{1}{n_h} \frac{\partial d}{\partial \boldsymbol{\nu}} \tag{A-13}$$

A.3.1. Yield function

By applying Eq. B-1 on $d = \langle \boldsymbol{\nu}, \boldsymbol{\chi} \rangle$, it is possible to define:

$$z(\mathbf{x}, \boldsymbol{\nu}, \theta) + w(\mathbf{x}, \boldsymbol{\chi}, \theta) = \langle \boldsymbol{\nu}, \boldsymbol{\chi} \rangle = d \tag{A-14}$$

where z and w are the force and flow potentials (Houlsby, 2014; Houlsby & Puzrin, 2007), respectively. Thus, the following properties apply (in accordance with Eq. B-2):

$$\boldsymbol{\chi} = \frac{\partial z(\mathbf{x}, \boldsymbol{\nu}, \theta)}{\partial \boldsymbol{\nu}}, \boldsymbol{\nu} = \frac{\partial w(\mathbf{x}, \boldsymbol{\chi}, \theta)}{\partial \boldsymbol{\chi}} \tag{A-15}$$

By comparing Eq. A-15 with Eq. A-13, it can be concluded that $\frac{\partial z}{\partial \boldsymbol{\nu}} = \frac{1}{n_h} \frac{\partial d}{\partial \boldsymbol{\nu}}$. For rate-independent materials, which are the motivation behind the model in this paper, the dissipation function is homogeneous of order one ($n_h=1$), which yields $z=d$. Further substitution into Eq. A-14 results in $w(\mathbf{x}, \boldsymbol{\chi}, \theta)=0$, which means that the flow potential is always zero. In this case, it is possible to derive a function of the forces that is identically zero when yielding occurs:

$$w(\mathbf{x}, \boldsymbol{\chi}, \theta) = Y' y(\mathbf{x}, \boldsymbol{\chi}, \theta) = 0 \tag{A-16}$$

where Y' is a non-zero value. Thus, $y(\mathbf{x}, \boldsymbol{\chi}, \theta)=0$, which is the yield function (Houlsby, 2014; Houlsby & Puzrin, 2002, 2007), defined in generalized force space (not in true stress space).

Appendix B. Legendre transforms

The Legendre transform has a wide range of applications, especially in thermodynamics. As an example, this transform may be invoked to interchange between different types of energy function; internal energy (*u*), enthalpy (*h*), Helmholtz free energy (*f*), and Gibbs free energy (*g*). Another example is the interchange between the dissipation and the yield functions for dissipative materials. Precisely, the purpose of this transform is to interchange the role of any independent variable of a function to its conjugate variable. Suppose that l_1 is an independent variable (active variable) of a set of variables that defines the function $k_1(l_1, a_1, a_2, a_3 \ldots)$. By Legendre transformation, the function k_1 is converted to the function k_2 which is defined by the same set of passive independent variables ($a_1, a_2, a_3, \ldots$); however, the active variable l_1 is replaced by its conjugate variable l_2, through application of the product-rule between the active variables ($<l_1 l_2>$). This can be mathematically shown as:

$$k_1(l_1, a_1, a_2, a_3, \ldots) + k_2(l_2, a_1, a_2, a_3, \ldots) = \langle l_1, l_2 \rangle \tag{B-1}$$

where $\langle \rangle$ is the inner product operator. This transform can be applied to any set of independent variables.

One of the important features of the Legendre transform is that the properties of one function remain unchanged during the transformation and the properties are transferred to the other function. This means that, in the case of applying the Legendre transform on an energy function, using other types of energy function would lead to the same results. With the same reasoning, invoking the Legendre transform for the dissipation function results in the interchangeable use of the yield function with the dissipation function.

The Legendre transform provides two important properties; one is related to the active variable(s) and the other is related to the passive variable(s). It can be proven that the partial differential of each function with respect to its corresponding active variable is equal to their corresponding conjugates. This can be shown as:

$$l_2 = \frac{\partial k_1(l_1, a_1, a_2, a_3, \ldots)}{\partial l_1}$$
$$l_1 = \frac{\partial k_2(l_2, a_1, a_2, a_3, \ldots)}{\partial l_2} \tag{B-2}$$

The partial differentials with respect to passive variables are identical for both functions:

$$\frac{\partial k_1(l_1, a_1, a_2, a_3, \ldots)}{\partial l_i} = \frac{\partial k_2(l_2, a_1, a_2, a_3, \ldots)}{\partial l_i}; i = 1, 2, 3, \ldots \tag{B-3}$$

This equation is the transfer of the properties of k_1 to k_2.

Appendix C. Properties of homogeneous functions

A function $r(e)$ is homogeneous of degree n_h with respect to all the values of *t* if the following statement stands:

$$r(te) = t^{n_h} r(e) \tag{C-1}$$

This definition can be generalized to any finite number of variables for the function. From the mathematical point of view, homogeneous functions possess a mapping (scaling) characteristic.

One of the properties of a homogeneous function, which is extensively implemented in thermodynamics, is that Euler's theorem applies. According to this theorem, if a function *r* is defined by a variable *e*, and is homogeneous to degree n_h, then such a function can be written in terms of its partial derivatives with respect to *e*:

$$n_h r(e) = \frac{\partial r(e)}{\partial e} e \tag{C-2}$$

Appendix D. Components of Eq. 22

The derivative components of the plastic multiplier in Eq. 22 are as follows:

$$\{\mathbf{r}\} = \begin{Bmatrix} r_p \\ r_q \end{Bmatrix} = 2 \begin{Bmatrix} B^2(p-C) - \beta A^2(q - \beta p) \\ A^2(q - \beta p) \end{Bmatrix} \tag{D-1}$$

$$\left\{ \frac{\partial y}{\partial \sigma} \right\} = \begin{Bmatrix} \dfrac{\partial y}{\partial p} \\ \dfrac{\partial y}{\partial q} \end{Bmatrix} = 2 \begin{Bmatrix} A(1-\gamma)\left((q-\beta p)^2 - B^2\right) + BM(1-\alpha)\left((p-C)^2 - A^2\right) + \left(B^2(p-C) - \beta A^2(q-\beta p)\right) \\ A^2(q - \beta p) \end{Bmatrix} \tag{D-2}$$

$$\left\{\frac{\partial y}{\partial \dot{\boldsymbol{\varepsilon}}^p}\right\} = \left\{\begin{matrix} \dfrac{\partial y}{\partial \dot{\varepsilon}_v^p} \\[2mm] \dfrac{\partial y}{\partial \dot{\varepsilon}_s^p} \end{matrix}\right\} = \left\{\begin{matrix} \left(\left(\dfrac{1+e_0}{\lambda-\kappa}\right)\gamma p_{cT}\right)\left(A\left((q-\beta p)^2 - B^2\right) + \alpha MB\left((p-C)^2 - A^2\right) - B^2(p-C)\right) \\[3mm] 0 \end{matrix}\right\} \tag{D-3}$$

$$\frac{\partial y}{\partial \theta} = \frac{\partial y}{\partial A}\frac{\partial A}{\partial p_{cT}}\frac{\partial p_{cT}}{\partial \theta} + \frac{\partial y}{\partial B}\frac{\partial B}{\partial p_{cT}}\frac{\partial p_{cT}}{\partial \theta} + \frac{\partial y}{\partial C}\frac{\partial C}{\partial p_{cT}}\frac{\partial p_{cT}}{\partial \theta} + \frac{\partial y}{\partial B}\frac{\partial B}{\partial M}\frac{\partial M}{\partial \theta} \rightarrow$$

$$\frac{\partial y}{\partial \theta} = (-\mu\gamma p_{cT})\left(A\left((q-\beta p)^2 - B^2\right) + \alpha MB\left((p-C)^2 - A^2\right) - B^2(p-C)\right)... \tag{D-4}$$

$$... + 2\pi B\left((p-C)^2 - A^2\right)\left((1-\alpha)p + \frac{\alpha\gamma}{2}p_{cT}\right)$$

Appendix E. Temperature dependent incremental formulations

E.1. Stress-controlled incremental formulation

In a stress-controlled condition, stress increments are imposed on the system as inputs and the resulting strain increments are calculated. Most geotechnical numerical simulations, e.g. foundation analyses, come under this category.

The total strain increment can be determined by differentiating Eqs. 5 and 6:

$$\left\{\begin{matrix} \dot{\varepsilon}_v \\ \dot{\varepsilon}_s \end{matrix}\right\} = \left\{\begin{matrix} \dot{\varepsilon}_v^e \\ \dot{\varepsilon}_s^e \end{matrix}\right\} + \left\{\begin{matrix} \dot{\varepsilon}_v^\theta \\ 0 \end{matrix}\right\} + \left\{\begin{matrix} \dot{\varepsilon}_v^p \\ \dot{\varepsilon}_s^p \end{matrix}\right\} \tag{E-1}$$

where the elastic strains are:

$$\dot{\varepsilon}_v^e = -\left(\frac{\partial^2 g_1(p,q)}{\partial p \partial p}\dot{p} + \frac{\partial^2 g_1(p,q)}{\partial p \partial q}\dot{q}\right)$$
$$\dot{\varepsilon}_s^e = -\left(\frac{\partial^2 g_1(p,q)}{\partial q \partial p}\dot{p} + \frac{\partial^2 g_1(p,q)}{\partial q \partial q}\dot{q}\right) \tag{E-2}$$

which can be rewritten in the compact form:

$$\left\{\begin{matrix} \dot{\varepsilon}_v^e \\ \dot{\varepsilon}_s^e \end{matrix}\right\} = [\mathbf{C}^e]\left\{\begin{matrix} \dot{p} \\ \dot{q} \end{matrix}\right\} = -\begin{bmatrix} \dfrac{\partial^2 g_1}{\partial p^2} & \dfrac{\partial^2 g_1}{\partial p \partial q} \\[3mm] \dfrac{\partial^2 g_1}{\partial q \partial p} & \dfrac{\partial^2 g_1}{\partial q^2} \end{bmatrix}\left\{\begin{matrix} \dot{p} \\ \dot{q} \end{matrix}\right\}$$

where $[\mathbf{C}^e]$ is the elastic compliance (or flexibility) matrix. With respect to Eq. 3 or Eq. 4, the components of the elastic compliance matrix can be derived, respectively, as:

$$[\mathbf{C}^e] = \frac{1}{3\overline{G}p_{ref}\left(\dfrac{p}{p_{ref}}\right)^n}\begin{bmatrix} \left(\dfrac{3\overline{G}}{\overline{K}}\left(\dfrac{p}{p_{ref}}\right)^{n-m} + \overline{n}\eta^2\right) & -n\eta \\[3mm] -n\eta & 1 \end{bmatrix}; \overline{n} = \frac{n(n+1)}{2} \tag{E-3}$$

$$[\mathbf{C}^e] = \frac{1}{3\overline{G}p_{ref}\left(\dfrac{p}{p_{ref}}\right)^n}\begin{bmatrix} \left(\dfrac{3\overline{G}}{\overline{K}}\left(\dfrac{p}{p_{ref}}\right)^{n-1} + \overline{n}\eta^2\right) & -n\eta \\[3mm] -n\eta & 1 \end{bmatrix} \tag{E-4}$$

The thermo-elastic strain increment is:

$$\dot{\varepsilon}_v^\theta = 3\alpha^* \dot{\theta} \tag{E-5}$$

The plastic strain increments, $\{\dot{\boldsymbol{\varepsilon}}^p\} = \dot{\Lambda}\{\mathbf{r}\}$, are easily calculated by Eqs. 19 and 22.

In summary, the total strain increments in a stress-controlled condition can be calculated as:

$$\{\dot{\boldsymbol{\varepsilon}}\} = [\mathbf{C}^e]\{\dot{\boldsymbol{\sigma}}\} + 3\alpha^* \begin{Bmatrix} 1 \\ 0 \end{Bmatrix} \dot{\theta} + \dot{\Lambda}\{\mathbf{r}\} \tag{E-6}$$

E.2. Strain-controlled incremental formulation

In some geotechnical applications, e.g. triaxial soil element tests, strains are applied to the soil specimen and the stress increments are measured. This condition, where the total strain is the input and the stress increment is the measured output, is called the strain-controlled condition.

The plastic multiplier in Eq. 22 is determined for stress-controlled increments, which should be modified to be strain-increment dependent. Multiplying both sides of Eq. E-6 by $\left(\left\{ \frac{\partial y}{\partial \boldsymbol{\sigma}} \right\}^{\mathrm{T}} [\mathbf{C}^e]^{-1} \right)$ results in:

$$\left\{ \frac{\partial y}{\partial \boldsymbol{\sigma}} \right\}^{\mathrm{T}} \{\dot{\boldsymbol{\sigma}}\} = \left\{ \frac{\partial y}{\partial \boldsymbol{\sigma}} \right\}^{\mathrm{T}} [\mathbf{C}^e]^{-1} \{\dot{\boldsymbol{\varepsilon}}\} - 3\alpha^* \left\{ \frac{\partial y}{\partial \boldsymbol{\sigma}} \right\}^{\mathrm{T}} [\mathbf{C}^e]^{-1} \dot{\theta} - \dot{\Lambda} \left\{ \frac{\partial y}{\partial \boldsymbol{\sigma}} \right\}^{\mathrm{T}} [\mathbf{C}^e]^{-1} \{\mathbf{r}\} \tag{E-7}$$

Recalling the consistency condition (Eq. 21) and comparing with Eq. E-7, similar terms can be identified. By substituting and applying algebraic operations, the plastic multiplier defined by total strain increments can be determined:

$$\dot{\Lambda} = \frac{\left\{ \frac{\partial y}{\partial \boldsymbol{\sigma}} \right\}^{\mathrm{T}} [\mathbf{D}^e]\{\dot{\boldsymbol{\varepsilon}}\} + \left(\frac{\partial y}{\partial \theta} - 3\alpha^* \left\{ \frac{\partial y}{\partial \boldsymbol{\sigma}} \right\}^{\mathrm{T}} [\mathbf{D}^e] \right) \dot{\theta}}{\left\{ \frac{\partial y}{\partial \boldsymbol{\sigma}} \right\}^{\mathrm{T}} [\mathbf{D}^e]\{\mathbf{r}\} - \left\{ \frac{\partial y}{\partial \dot{\boldsymbol{\varepsilon}}^p} \right\}^{\mathrm{T}} \{\mathbf{r}\}} \tag{E-8}$$

where $[\mathbf{D}^e]$ is the elastic stiffness matrix and is the inverse of the elastic flexibility matrix $[\mathbf{C}^e]$ (Eq. E-3 and Eq. E-4, respectively):

$$[\mathbf{D}^e] = [\mathbf{C}^e]^{-1} = \frac{3\overline{GK}p_{ref}\left(\frac{p}{p_{ref}}\right)^m}{3\overline{G} + \overline{n}\eta^2\overline{K}\left(\frac{p}{p_{ref}}\right)^{m-n}} \begin{bmatrix} 1 & n\eta \\ n\eta & \left(\frac{3\overline{G}}{\overline{K}}\left(\frac{p}{p_{ref}}\right)^{n-m} + \overline{n}\eta^2 \right) \end{bmatrix}; \quad \overline{n} = \frac{n(1-n)}{2} \tag{E-9}$$

$$[\mathbf{D}^e] = \frac{3\overline{GK}p}{3\overline{G} + \overline{n}\overline{K}\eta^2\left(\frac{p}{p_{ref}}\right)^{1-n}} \begin{bmatrix} 1 & n\eta \\ n\eta & \left(\frac{3\overline{G}}{\overline{K}}\left(\frac{p}{p_{ref}}\right)^{n-1} + \overline{n}\eta^2 \right) \end{bmatrix} \tag{E-10}$$

By the use of Eq. E-6, the stress increments can be calculated from strain increments:

$$\{\dot{\boldsymbol{\sigma}}\} = [\mathbf{D}^e]\left(\{\dot{\boldsymbol{\varepsilon}}\} - 3\alpha^* \begin{Bmatrix} 1 \\ 0 \end{Bmatrix} \dot{\theta} - \dot{\Lambda}\{\mathbf{r}\} \right) \tag{E-11}$$

where $[\mathbf{D}^e]$ and $\dot{\Lambda}$ are calculated respectively from Eq. E-8 and Eq. E-9 (or E-10).

References

Abuel-Naga, H. M., Bergado, D. T., & Bouazza, A. (2007a). Thermally induced volume change and excess pore water pressure of soft Bangkok clay. *Engineering Geology, 89*, 144–154. https://doi.org/10.1016/j.enggeo.2006.10.002

Abuel-Naga, H. M., Bergado, D. T., Bouazza, A., & Ramana, G. V. (2007b). Volume change behaviour of saturated clays under drained heating conditions: experimental results and constitutive modeling. *Canadian Geotechnical Journal, 44*(8), 942–956. https://doi.org/10.1139/t07-031

Abuel-Naga, H. M., Bergado, D. T., & Lim, B. F. (2007c). Effect of temperature on shear strength and yielding behavior of soft Bangkok clay. *Soils and Foundations, 47*(3), 423–436. https://doi.org/10.3208/sandf.47.423

Abuel-Naga, H. M., Bergado, D. T., Ramana, G. V., Grino, L., Rujivipat, P., & Thet, Y. (2006). Experimental evaluation of engineering behavior of soft Bangkok clay under elevated temperature. *Journal of Geotechnical and Geoenvironmental Engineering, 132*(7), 902–910. https://doi.org/10.1061/(ASCE)1090-0241(2006)132:7(902

Addison, S. R. (1991). Homogenous functions in thermodynamics. *Proceedings Arkansas Academy of Science, 45*, 114–117.

Aung, Y., Khabbaz, H., & Fatahi, B. (2019). Mixed hardening hyper-viscoplasticity model for soils incorporating non-linear creep rate – H-creep model. *International Journal of Plasticity, 120*, 88–114. https://doi.org/10.1016/j.ijplas.2019.04.013

Bai, B., & Su, Z. (2012). Thermal responses of saturated silty clay during repeated heating–cooling processes. *Transport in Porous Media, 93*(1), 1–11. https://doi.org/10.1007/s11242-012-9939-6

Bathe, K. J., Ramm, E., & Wilson, E. L. (1975). Finite element formulations for large deformation dynamic analysis. *International Journal for Numerical Methods in Engineering, 9*(2), 353–386. https://doi.org/10.1002/nme.1620090207

Brandl, H. (2006). Energy foundations and other thermo-active ground structures. *Géotechnique, 56*(2), 81–122. https://doi.org/10.1680/geot.2006.56.2.81

Cekerevac, C., & Laloui, L. (2004). Experimental study of thermal effects on the mechanical behaviour of a clay. *International Journal for Numerical and Analytical Methods in Geomechanics, 28*(3), 209–228. https://doi.org/10.1002/nag.332

Churaev, N. V., Sobolev, V. D., & Zorin, Z. M. (1971). Measurement of viscosity of liquids in quartz capilaries. *Special Discussion on Thin Liquid Films and Boundary Layers* (pp. 213–220). New York: Academic Press.

Coccia, C. J. R., & McCartney, J. S. (2012). A thermo-hydro-mechanical true triaxial cell for evaluation of the impact of anisotropy on thermally induced volume changes in soils. *Geotechnical Testing Journal, 35*(2), Article 103803. https://doi.org/10.1520/GTJ103803

Collins, I. F. (2002). Associated and non-associated aspects of the constitutive laws for coupled elastic/plastic materials. *International Journal of Geomechanics, 2*(2), 259–267. https://doi.org/10.1061/(ASCE)1532-3641(2002)2:2(259)

Collins, I. F., & Hilder, T. (2002). A theoretical framework for constructing elastic/plastic constitutive models of triaxial tests. *International Journal for Numerical and Analytical Methods in Geomechanics, 26*(13), 1313–1347. https://doi.org/10.1002/nag.247

Collins, I. F., & Houlsby, G. T. (1997). Application of thermo-mechanical principles to the modeling of geo-materials. In *, 453. Proceedings: Mathematical, Physical and Engineering Sciences* (pp. 1975–2001). JSTOR. Retrieved from http://www.jstor.org/stable/53033.

Coombs, W. M., Crouch, R. S., & Augarde, C. E. (2013). A unique Critical State two-surface hyper-plasticity model for fine-grained particulate media. *Journal of the Mechanics and Physics of Solids, 61*(1), 175–189. https://doi.org/10.1016/j.jmps.2012.08.002

Cui, W., Potts, D. M., Zdravković, L., Gawecka, K. A., & Taborda, D. M. G. (2018). An alternative coupled thermo-hydro-mechanical finite element formulation for fully saturated soils. *Computers and Geotechnics, 94*, 22–30. https://doi.org/10.1016/j.compgeo.2017.08.011

Cui, Y. J., Sultan, N., & Delage, P. (2000). A thermo-mechanical model for saturated clays. *Canadian Geotechnical Journal, 37*(3), 607–620. https://doi.org/10.1139/t99-111

Dafalias, Y. F., & Taiebat, M. (2013). Anatomy of rotational hardening in clay plasticity. *Géotechnique, 63*(16), 1406–1418. https://doi.org/10.1680/geot.12.P.197

Dafalias, Y. F., & Taiebat, M. (2014). Rotational hardening with and without anisotropic fabric at critical state. *Géotechnique, 64*(6), 507–511. https://doi.org/10.1680/geot.13.T.035

Darabi, M. K., Al-Rub, Abu, R. K., & Omidi, O (2018). A thermodynamically consistent framework to derive local/nonlocal generalized non-associative plasticity/visco plasticity theories. *International Journal of Plasticity, 110*, 19–37. https://doi.org/10.1016/j.ijplas.2018.06.006

Deryaguin, B. V. (1986). *Theory of Stability of Colloids and Thin Films*. Moscow: Nauka.

Deryaguin, B. V., & Churaev, N. V. (1972). The isotherm of disjoining pressure of water films on quartz surface. *Dokl AN USSR, 207*(3), 572–575.

Deryaguin, B. V., & Churaev, N. V. (1984). *Wetting Films*. Moscow: Nauka.

Deryaguin, B. V., Churaev, N. V., & Muller, V. M. (1985). *Surface Forces*. Moscow: Nauka.

Di Donna, A., & Laloui, L. (2015). Response of soil subjected to thermal cyclic loading: experimental and constitutive study. *Engineering Geology, 190*, 65–76. https://doi.org/10.1016/j.enggeo.2015.03.003

Einav, I., & Puzrin, A. M. (2004). Pressure-dependent elasticity and energy conservation in elasto-plastic models for soils. *Journal of Geotechnical and Geoenvironmental Engineering, 130*(1), 81–92. https://doi.org/10.1061/(ASCE)1090-0241(2004)130:1(81)

Ghahremannejad, B. (2003). *Thermo-Mechanical Behavior of Two Reconstituted Clays*. PhD thesis, University of Sydney.

Golchin, A., & Lashkari, A. (2014). A critical state sand model with elastic–plastic coupling. *International Journal of Solids and Structures, 51*(15–16), 2807–2825. https://doi.org/10.1016/j.ijsolstr.2014.03.032

Graham, J., Tanaka, N., Crilly, T., & Alfaro, M. (2001). Modified Cam-Clay modeling of temperature effects in clays. *Canadian Geotechnical Journal, 38*(3), 608–621. https://doi.org/10.1139/t00-125

Hamidi, A., Tourchi, S., & Kardooni, F. (2017). A critical state based thermo-elasto-plastic constitutive model for structured clays. *Journal of Rock Mechanics and Geotechnical Engineering, 9*(6), 1094–1103. https://doi.org/10.1016/j.jrmge.2017.09.002

Hamidi, A., Tourchi, S., & Khazaei, C. (2015). Thermo-mechanical constitutive model for saturated clays based on critical state theory. *International Journal of Geomechanics, 15*(1), Article 04014038. https://doi.org/10.1061/(ASCE)GM.1943-5622.0000402

Hong, P. Y., Pereira, J. M., Cui, Y. J., & Tang, A. M. (2016). A two-surface thermo mechanical model for saturated clays. *International Journal for Numerical and Analytical Methods in Geomechanics, 40*(7), 1059–1080. https://doi.org/10.1002/nag.2474

Hong, P. Y., Pereira, J. M., Tang, A. M., & Cui, Y. J. (2013). On some advanced thermo-mechanical models for saturated clays. *International Journal for Numerical and Analytical Methods in Geomechanics, 37*(17), 2952–2971. https://doi.org/10.1002/nag.2170

Houlsby, G. T. (1997). The work input to a granular material. *Géotechnique, 47*(1), 193–196. https://doi.org/10.1680/geot.1997.47.1.193

Houlsby, G. T. (2014). Dissipation rate functions, pseudopotentials, potentials and yield surfaces. In R. C. Dewar, C. H. Lineweaver, R. K. Niven, & K. Regenauer-Lieb (Eds.), *Beyond the Second Law: Entropy Production and Non-equilibrium Systems* (pp. 73–95). Berlin, Heidelberg: Springer Berlin Heidelberg. https://doi.org/10.1007/978-3-642-40154-1_4.

Houlsby, G. T., Amorosi, A., & Rojas, E. (2005). Elastic moduli of soils dependent on pressure: a hyperelastic formulation. *Géotechnique, 55*(5), 383–392. https://doi.org/10.1680/geot.2005.55.5.383

Houlsby, G. T., & Puzrin, A. M. (2000). A thermo-mechanical framework for constitutive models for rate-independent dissipative materials. *International Journal of Plasticity, 16*(9), 1017–1047. https://doi.org/10.1016/S0749-6419(99)00073-X

Houlsby, G. T., & Puzrin, A. M. (2002). Rate-dependent plasticity models derived from potential functions. *Journal of Rheology, 46*(1), 113–126. https://doi.org/10.1122/1.1427911

Houlsby, G. T., & Puzrin, A. M. (2007). Principles of Hyper-Plasticity: An Approach to Plasticity Theory based on Thermodynamic Principles. *Principles of Hyper-Plasticity: an approach to plasticity theory based on thermodynamic principles*. London: Springer. https://doi.org/10.1007/978-1-84628-240-9

Hueckel, T., & Baldi, G. (1991). Thermo-plasticity of saturated clays: experimental constitutive study. *Journal of Geotechnical Engineering, 116*(12), 1778–1796.

Hueckel, T., François, B., & Laloui, L. (2009). Explaining thermal failure in saturated clays. *Géotechnique, 59*(3), 197–212. https://doi.org/10.1680/geot.2009.59.3.197

Israelachvili, J. N., & Pashley, R. M. (1983). Molecular layering of water at surfaces and origin of repulsive hydration forces. *Nature, 306*(5940), 249–250. https://doi.org/10.1038/306249a0

Khalili, N., Uchaipichat, A., & Javadi, A. A. (2010). Skeletal thermal expansion coefficient and thermo-hydro-mechanical constitutive relations for saturated homogeneous porous media. *Mechanics of Materials, 42*(6), 593–598. https://doi.org/10.1016/j.mechmat.2010.04.001

Kuntiwattanakul, P., Towhata, I., Ohishi, K., & Seko, I. (1995). Temperature effects on undrained characteristics of clay. *Soils and Foundation, 35*(1), 147–162. https://doi.org/10.3208/sandf1972.35.147

Lai, Y., Liao, M., & Hu, K. (2016). A constitutive model of frozen saline sandy soil based on energy dissipation theory. *International Journal of Plasticity, 78*, 84–113. https://doi.org/10.1016/j.ijplas.2015.10.008

Laloui, L., & Cekerevac, C. (2003). Thermo-plasticity of clays: an isotropic yield mechanism. *Computers and Geotechnics, 30*(8), 649–660. https://doi.org/10.1016/j.compgeo.2003.09.001

Laloui, L., & Cekerevac, C. (2008). Non-isothermal plasticity model for cyclic behavior of soils. *International Journal for Numerical and Analytical Methods in Geomechanics, 32*(5), 437–460. https://doi.org/10.1002/nag.629

Laloui, L., Cekerevac, C., & François, B. (2005). Constitutive modeling of the thermo-plastic behavior of soils. *Revue Européenne de Génie Civil, 9*(5–6), 635–650. https://doi.org/10.1080/17747120.2005.9692774

Laloui, L., & François, B. (2009). ACMEG-T: soil thermo-plasticity model. *Journal of Engineering Mechanics, 135*(9), 932–944. https://doi.org/10.1061/(ASCE)EM.1943-7889.0000011

Laloui, L., Leroueil, S., & Chalindar, S. (2008). Modeling the combined effect of strain rate and temperature on one-dimensional compression of soils. *Canadian Geotechnical Journal, 45*(12), 1765–1777. https://doi.org/10.1139/T08-093

Lashkari, A., & Golchin, A. (2014). On the influence of elastic–plastic coupling on sands response. *Computers and Geotechnics, 55*, 352–364. https://doi.org/10.1016/j.compgeo.2013.09.016

Ma, Q. J., Ng, C. W. W., Mašín, D., & Zhou, C. (2017). An approach for modelling volume change of fine-grained soil subjected to thermal cycles. *Canadian Geotechnical Journal, 54*(6), 896–901. https://doi.org/10.1139/cgj-2016-0459

Mašín, D., & Khalili, N. (2012). A thermo-mechanical model for variably saturated soils based on hypoplasticity. *International Journal for Numerical and Analytical Methods in Geomechanics, 36*(12), 1461–1485. https://doi.org/10.1002/nag.1058

Mitchell, J. K., & Soga, K. (2005). *Fundamentals of Soil Behavior*. John Wiley & Sons.

Ng, C. W. W., Cheng, Q., Zhou, C., & Alonso, E. E. (2016). Volume changes of an unsaturated clay during heating and cooling. *Géotechnique Letters, 6*(3), 192–198. https://doi.org/10.1680/jgele.16.00059

Nieto-Leal, A., Kaliakin, V. N., & Mashayekhi, M. (2018). Improved rotational hardening rule for cohesive soils and definition of inherent anisotropy. *International Journal for Numerical and Analytical Methods in Geomechanics, 42*(3), 469–487. https://doi.org/10.1002/nag.2750

Osipov, V. I. (2015). *Physicochemical Theory of Effective Stress in Soils (Vol. 41)*. Cham: Springer International Publishing. https://doi.org/10.1007/978-3-319-20639-4

Özdemir, I., Brekelmans, W. A. M., & Geers, M. G. D. (2008). Computational homogenization for the thermo-mechanical analysis of heterogeneous solids. *Computer Methods in Applied Mechanics and Engineering, 198*(3–4), 602–613. https://doi.org/10.1016/j.cma.2008.09.008

Perevertaev, V. D., & Metsik, M. S. (1966). Investigation of water vapor adsorption on mica crystal surface. *Colloidal Journal, 28*(2), 254–259.

Puzrin, A. M. (2012). *Constitutive Modelling in Geomechanics*. Berlin: Heidelberg: Springer Berlin Heidelberg. https://doi.org/10.1007/978-3-642-27395-7

Rajagopal, K. R., & Srinivasa, A. R. (2019). Some remarks and clarifications concerning the restrictions placed on thermodynamic processes. *International Journal of Engineering Science, 140*, 26–34. https://doi.org/10.1016/j.ijengsci.2019.04.003

Sedighi, M., & Thomas, H. R. (2014). Micro porosity evolution in compacted swelling clays — a chemical approach. *Applied Clay Science, 101*, 608–618. https://doi.org/10.1016/j.clay.2014.09.027

Srinivasa, A. R. (2010). Application of the maximum rate of dissipation criterion to dilatant, pressure dependent plasticity models. *International Journal of Engineering Science, 48*(11), 1590–1603. https://doi.org/10.1016/j.ijengsci.2010.09.010

Sultan, N., Delage, P., & Cui, Y. J. (2002). Temperature effects on the volume change behavior of Boom clay. *Engineering Geology, 64*, 135–145. https://doi.org/10.1016/S0013-7952(01)00143-0

Tanaka, N., Graham, J., & Crilly, T. (1997). Stress-strain behavior of reconstituted illitic clay at different temperatures. *Engineering Geology, 47*(4), 339–350. https://doi.org/10.1016/S0013-7952(96)00113-5

Terzaghi, K. (1925). *Erdbaumechanik auf Bodenphysikalischer Grundlage*. Liepzig-Vienna: Franz Deuticke.

Thomas, H. R., Vardon, P. J., & Cleall, P. J. (2014). Three-dimensional behavior of a prototype radioactive waste repository in fractured granitic rock. *Canadian Geotechnical Journal, 51*(3), 246–259. https://doi.org/10.1139/cgj-2013-0094

Towhata, I., Kuntiwattanaku, P., Seko, I., & Ohishi, K. (1993). Volume change of clays induced by heating as observed in consolidation tests. *Soils and Foundations, 33*(4), 170–183. https://doi.org/10.3208/sandf1972.33.4_170

Uchaipichat, A., & Khalili, N. (2009). Experimental investigation of thermo-hydro-mechanical behavior of an unsaturated silt. *Géotechnique, 59*(4), 339–353. https://doi.org/10.1680/geot.2009.59.4.339

Vega, A., & McCartney, J. S. (2015). Cyclic heating effects on thermal volume change of silt. *Environmental Geotechnics, 2*(5), 257–268. https://doi.org/10.1680/envgeo.13.00022

Wheeler, S. J., Näätänen, A., Karstunen, M., & Lojander, M. (2003). An anisotropic elasto-plastic model for soft clays. *Canadian Geotechnical Journal, 40*(2), 403–418. https://doi.org/10.1139/t02-119

Xiong, Y., Ye, G., Zhu, H., Zhang, S., & Zhang, F. (2016). Thermo-elasto-plastic constitutive model for unsaturated soils. *Acta Geotechnica, 11*(6), 1287–1302. https://doi.org/10.1007/s11440-016-0462-8

Yao, Y. P., & Zhou, A. N. (2013). Non-isothermal unified hardening model: a thermo-elasto-plastic model for clays. *Géotechnique, 63*(15), 1328–1345. https://doi.org/10.1680/geot.13.P.035

Zhou, C., Fong, K. Y., & Ng, C. W. W. (2017). A new bounding surface model for thermal cyclic behavior. *International Journal for Numerical and Analytical Methods in Geomechanics, 41*, 1656–1666. https://doi.org/10.1002/nag.2688

Zhou, C., & Ng, C. W. W. (2015). A thermo-mechanical model for saturated soil at small and large strains. *Canadian Geotechnical Journal, 52*(8), 1101–1110. https://doi.org/10.1139/cgj-2014-0229

Zhou, C., & Ng, C. W. W. (2016). Simulating the cyclic behavior of unsaturated soil at various temperatures using a bounding surface model. *Géotechnique, 66*(4), 344–350. https://doi.org/10.1680/jgeot.15.P.001

Zhou, C., Xu, J., & Ng, C. W. W. (2015). Effects of temperature and suction on secant shear modulus of unsaturated soil. *Géotechnique Letters, 5*, 123–128. https://doi.org/10.1680/geolett.14.00096

Ziegler, H. (1977). An introduction to thermomechanics. *North-Holland Publishing Co. (North-Holland Series in Applied Mathematics and Mechanics. Volume 21), Amsterdam: Amsterdam*.

Zorin, Z. M., Sobolev, V. D., & Churaev, N. V. (1972). Variation of capillary pressure, surface tension, and liquid viscosity in quartz micro-capillaries. *Surface Forces in Thin Films and Disperse Systems*. Moscow: Nauka.